

SOLUTION CHEMISTRY EFFECTS ON CORROSION OF CARBON STEELS IN PRESENCE OF CO₂ AND ACETIC ACID

Egil Gulbrandsen
Institute for Energy Technology
Instituttveien 18
NO-1254 Kjeller, Norway

Katerina Bilkova
Institute for Energy Technology
Instituttveien 18
NO-1254 Kjeller, Norway

ABSTRACT

The corrosion behavior of X65 pipeline steel in solutions containing carbon dioxide (CO₂), acetic acid (CH₃COOH, abbreviated HAc) and 0.1-0.3 % sodium chloride (NaCl) was investigated on rotating cylinder specimens in glass cells. The tests were carried out at 25 °C (1 bar CO₂) and 80 °C (0.5 bar CO₂). The initial concentration of HAc was varied between 0 and 600 ppm (0-10 mM). The ferrous ion (Fe²⁺) concentration was in most of the tests held far below the iron carbonate (FeCO₃) saturation limit. The electrode rotation rate was 1900 RPM, corresponding to ca. 1 m/s peripheral velocity. At 25 °C the HAc inhibited general corrosion, but promoted formation of deep corrosion pits. At 80 °C the corrosion was uniform; the corrosion rates were high (several tens of mm/y) in presence of HAc.

The literature on CO₂ corrosion in presence of HAc was reviewed. Some studies reported increased corrosivity in presence of HAc, whereas others reported that HAc works as an inhibitor. Most of the corrosion data reported in the literature was, however, found to be consistent when the effect of temperature and type of corrosion attack observed in the present work was taken into consideration. The literature data indicated that HAc corrosion could be mitigated by means of corrosion inhibitors and pH control. The physiochemical properties of HAc was also reviewed: diffusion coefficient, partial pressure of HAc over aqueous HAc solutions, HAc solubility in oil, and formation constants of ferrous and calcium acetate complexes. The effect of complex formation was investigated and discussed.

Key words: acetic acid, carbon dioxide, corrosion, carbon steel, solution chemistry

INTRODUCTION

Short chain carboxylic acids are often present in oil and gas reservoirs beside other corrosive compounds like carbon dioxide (CO₂) and hydrogen sulfide (H₂S). Amongst these short chain acids, acetic acid (CH₃COOH, abbreviated HAc) appears to be the most abundant. The effect of HAc on the corrosion of mild steel in sweet systems has been the subject of a number of experimental studies during the last few years, see summary below. It appears that HAc can give a significant contribution to the overall corrosion rate, and raise the uninhibited corrosion rate to several tens of millimeters per year. The worst-case corrosion rates are obviously unacceptable in the field, and robust corrosion mitigation techniques are needed. However, the introduction of the inhibitor availability concept¹⁻⁵ justifies studying worst-case corrosion rates, since the corrosion during periods of inhibitor unavailability may contribute significantly to the loss of pipe wall thickness. Furthermore, the study of worst-case corrosion rates may contribute to the understanding of the corrosion mechanisms, and the development of corrosion prediction model tools.

The present paper reports the results of a laboratory study on the effect of HAc under conditions without protective corrosion films at two temperatures, 25°C and 80 °C. The tests focus on the bottom-of-line corrosion in gas-condensate pipeline conditions. The objective of the work was to assess the effect of HAc on the potential (worst case) corrosiveness in such systems, and to generate data that may facilitate corrosion prediction in presence of HAc. Furthermore, the paper contains a brief summary of the literature on the effect of HAc on corrosion in oil- and gas production and transportation systems. The aim was to extract relevant information and clear up some apparent inconsistencies in the literature. For example, some reports state that HAc increases corrosion, while others state that HAc acts as an anodic inhibitor. Physio-chemical data of HAc were also reviewed. Corrosion tests examining the effect of HAc on protective corrosion films were also performed in the same project. Those results will be reported at a later stage.

LITERATURE REVIEW

Corrosion data

The present summary covers the literature from 1983 until today. Crolet et al.⁶ and Dougherty⁷ provided summaries of the early literature on the role of HAc on corrosion in oil- and gas wells. In brief, the effect of short chain carboxylic acids was studied already in the 1940's, but the subject received little attention until it was brought up again in the 1980's.⁸⁻¹⁰ Ref. 7 also includes parts of the recent literature on the effect of HAc. The subject has also been given some attention in a recent review of CO₂ corrosion.¹¹

Bonis and Crolet published a systematic investigation of Elf's field experience with respect to HAc and other parameters.^{9,10} Corrosion data from a number of wells were classified according to the following definitions:

- Non-corrosive: wells where no corrosion problems had been encountered over a period of at least 8 years, in spite of significant water cut
- Corrosive: wells where corrosion problems had been encountered, with inadequate lifetimes, generally less than 2-3 years
- Possibly corrosive: wells where the absence of corrosion problems could not be considered to be definitive (e.g. due to low water cut)

It was found that a number of wells were non-corrosive even if the potential corrosivity was high. On the other hand, the majority of the corrosive wells had HAC contents above ca. 1 mM (60 ppm). A number of predictive rules were established.⁹⁻¹⁰ Both for gas and oil wells it was concluded that undissociated HAC concentrations higher than 0.1-1 mM was a critical factor for corrosion.

The corrosion failures were always caused by localized attack (mesa type of attack). The authors list the following conditions for high corrosion rates:

1. Water wetting of the pipe wall. The localized corrosion attack, however, is not only caused by localized water wetting, since mesa attack also occurs in pure aqueous CO₂ systems.
2. High potential corrosivity (high P_{CO2}, low pH etc.)
3. Conditions favorable for localized attack. It is pointed out that localized corrosion necessarily involves surface deposits (protecting the surrounding areas, but not in the localized attack).

Crolet and Bonis⁸ discussed the role of HAC on the in-situ pH. It was pointed out that routine analysis of alkalinity will not differentiate between acetate (Ac⁻) and bicarbonate (HCO₃⁻), and the calculated pH will be in error. Their experimental data showed that HAC increased the cathodic limiting currents, and thus could increase the potential corrosiveness.⁸ The different equilibria involved in the CO₂ – HAC system were discussed in great detail in a recent paper from the same authors.¹²

Hedges and McVeigh¹³ tested the effect of HAC on CO₂ corrosion at 60 °C (0.8 bar CO₂, 3% NaCl and synthetic formation water). The corrosion rates increased with increasing HAC concentration. However, the pH was not adjusted, and the solution not replenished during the test. This caused decreasing corrosion rates with time as the HAC was depleted by the corrosion. The corrosion rate increased again when more HAC was added to the cell. Furthermore, adding Ac⁻ to a CO₂ system increased the corrosion rates, even if the pH increased. These results can be explained by the fact that some Ac⁻ is converted to HAC by the acidity of CO₂. It was also pointed out that Ac⁻ may be counted as HCO₃⁻ in routine analysis, leading to too high pH estimates, and hence under-prediction of the corrosivity.

Crolet, Thevenot and Dugstad⁶ investigated the effect of HAC on the anodic dissolution of carbon steel under CO₂ and N₂ atmospheres. (Room temperature, 1 bar CO₂, 0.2 M NaClO₄ brine,). The anodic part-reaction was inhibited by HAC. This was inferred from the shift of the anodic Tafel curve to more positive potentials. The anodic reaction orders with respect to total acetate ([HAc] + [Ac⁻]) were reported. It was found that the corrosion rate was slightly inhibited above ca. 3 mM (180 ppm) HAC. Furthermore, it was found that the corrosion rate remained high when the HAC was continuously replenished in corrosion tests at 50°C, 1 bar CO₂, pH 5.2).

Ueda and Takabe¹⁴ investigated the effect of 0.5 % (5000 ppm) HAC on carbon and chromium bearing steels at 60-300 °C. (Autoclave test, 30 bar CO₂, 5 % NaCl, stirring, mass loss measurements). They found that the corrosion rate was considerably higher with HAC than with only CO₂. Exception was at 60 °C, where HAC gave lower corrosion rate. This may be related to the anodic inhibition observed in ref. 6.

Tebbal and Hackermann¹⁵⁻¹⁶ tested the effect of formic acid, acetic acid and chloroacetic acid on the pitting corrosion rate. (Room temperature, 0-17 mM acid). It was concluded that formic acid and

acetic acid inhibited pitting, chloroacetic acid had no effect. The definition of pits applied in these studies is uncertain, however, given the high number of pits reported for the pure CO₂ system (100 pits/mm²).¹⁵

Dugstad and co-workers¹⁷ tested the effect of 12 ppm undissociated HAc under film forming conditions at 80 °C. (Flow loop, 2 bar CO₂, pH 5.8, 6-30 ppm Fe²⁺ (i.e. supersaturated), 0.1 % NaCl. The total amount of acetic species was 90-120 ppm. The corrosion attack varied considerably between the different steels tested. However, it was concluded that the HAc caused more mesa attack (high number of small attacks). The corrosion films were more fragmented, with more pores and flaws. In some cases a protective corrosion film did not form at all. The localized corrosion was more severe at high flow rates.

The effect of HAc has been studied over a wide range of conditions in a series of recent papers from Ohio University.¹⁸⁻²⁴ Sun et al.¹⁸ used rotating cylinder specimens in glass cells bubble tests to investigate the effect of HAc on the part reactions under N₂ and CO₂ atmospheres at room temperature (0-1000 ppm (0-17 mM) HAc, 3 wt-% NaCl). Polarization curves showed that HAc increased the cathodic current, and that the H₂ evolution from HAc was activation controlled at room temperature. HAc inhibited the anodic part reaction. The electrochemically measured corrosion rates in short term tests (< 1 hr.) showed no significant variation with HAc concentration.

George et al.¹⁹ used basically the same setup as Sun et al.¹⁸ to further study the effect HAc on the corrosion rate in the temperature range 22-60 °C (0-1000 ppm HAc, 3 wt-% NaCl), and developed an electrochemical/hydrodynamic model for the cathodic reaction taking into account the reduction of H⁺ (from the bulk of the solution), H₂CO₃, and HAc. The anodic reaction was modeled by means Tafel equations obtained from the experimental data. The corrosion rates were studied by mass loss measurements (24 hrs exposure). The mass loss rates increased substantially with HAc concentration at 40 °C and 60 °C, but not at 22 °C. It was observed that the cathodic current in presence of HAc was reduced in a synthetic brine with high salt contents compared to 3 wt-% NaCl. The mass loss data showed no significant difference between them. The de Waard model was extended to take HAc into account. In following papers Wang et al.²⁰ and George et al.²¹ extended the previous experimental work to corrosion loops at higher CO₂ partial pressures. It was noted that the anodic inhibition observed at room temperature was lifted at 60 °C.

Singer et al.²² studied top-of-line corrosion in presence of HAc and CO₂ (70 °C, 0-1000 ppm HAc). The corrosion rate in the top of the line increased gradually with increasing HAc concentration and with increasing condensation rates, but the rates were substantially lower than in the bottom of the line. Localized attack was observed in the bottom but not in the top of the line. In a subsequent paper, Méndez et al.²³ extended the work to include effect of glycol and pH control. In general, little effect of HAc was observed on the top-of-line corrosion rate in these tests (2-3 days exposure).

Nafday and Nestic²⁴ studied the effect of HAc on FeCO₃ corrosion product film protectiveness at 80 °C in 3 wt-% NaCl under 0.5 bar CO₂. The concentrations of undissociated HAc was 0-180 ppm. The tests were carried out at relative FeCO₃ supersaturations equal to 32 and 162. No significant effect of HAc on FeCO₃ layer protectiveness or morphology was found in any of the tests. The corrosion film growth rate, inferred from the rate of decrease of corrosion rate, was determined by the supersaturation.

Gunalton and co-workers²⁵⁻²⁶ correlated field cases of top-of-line corrosion to the water condensation rate as the most important factor. Furthermore, high concentrations of organic acids were

present in some of the lines (250-3000 ppm HAc). It was demonstrated experimentally²⁶ that the corrosion was severely affected by the presence of organic acids in this concentration range.

Guo et al.²⁷ studied the effect of HAc and Ac^- (50 °C, 1 bar CO_2 , and 100 °C, 10 bar CO_2). The polarization curves showed increased cathodic currents, and some indication of inhibition of the anodic reaction with increasing HAc concentration (0-360 ppm).

Garber et al.⁵³⁻⁵⁴ developed computer models to calculate downhole pH in presence of CO_2 and organic acids, and suggested to correlate corrosion and scaling tendency to deviation in pH from FeCO_3 saturation pH.

The effect of HAc on corrosion of iron and steel has also been investigated in a few more fundamental studies:

Hurlen et al.²⁸ investigated the effect of acetate buffers on the cathodic reaction on iron (N_2 atmosphere, 25 °C). They observed a limiting cathodic current that was dependent on stirring and HAc concentration. However, in the potential region of activation controlled reaction the HAc had no (or negligible) effect. This was interpreted as an indication that HAc is not a direct reactant in the H_2 evolution reaction.

Bech-Nielsen²⁹ investigated the effect of HAc and Ac^- on the anodic part reaction on iron (25 °C, N_2 atmosphere, pH 4, 1 M NaClO_4 solution). Inhibition of the anodic part reaction was observed also in this work. The reaction order of the anodic reaction with respect to Ac^- was -0.7.

Garsany et al.³⁰⁻³³ used voltametry to study the effect of HAc on the cathodic part reaction on platinum and steel in CO_2 environment (25 and 60 °C). They observed a limiting cathodic current in HAc solutions; the magnitude of the limiting current was proportional to the HAc concentration, and proportional to square root of the rotating disc rotation rate. This shows that the limitation is caused by the diffusion of HAc. The data could not differentiate between direct reduction of HAc and reduction of H^+ after dissociation, since the dissociation reaction is very fast. In solutions with both HAc and CO_2 present the cathodic limiting current was the sum of the individual contributions of diffusion limited reduction of solution equilibrium protons, diffusion limited reduction of HAc, and reaction limited reduction of H_2CO_3 . The relative importance of these reactions depends, amongst many factors, on convection, temperature and concentration of the involved species. The reduction currents of bicarbonate (HCO_3^-) and water (H_2O) were negligible, since they are so poor proton donors (low dissociation constants). Direct reduction of CO_2 is also negligible. The importance of proper speciation, including consideration of ion activities, was pointed out. References 32-33 give a good description of all the equilibria and reactions involved. The potential region of the diffusion-limited reduction of HAc on carbon steel was much lower than the normal corrosion potential in CO_2 corrosion. The HAc reduction is therefore activation controlled under CO_2 corrosion conditions. It was also found that the anodic currents were influenced by the presence of HAc or Ac^- . This was attributed to different properties of the corrosion products films. The works of Garsany et al.³⁰⁻³³ also contain references to previous fundamental work on the electrochemical reduction of HAc and other weak organic acids.

Corrosion mitigation in presence of HAc

Relatively few studies have been reported on corrosion inhibition in systems containing CO_2 and HAc.^{13, 26, 35- 39} These studies concluded that the corrosion in presence of CO_2 and HAc could be

inhibited. However, increased inhibited corrosion rates and/or localized corrosion attacks were observed in the presence of HAc with some inhibitors.³⁶⁻³⁸ Careful selection of inhibitors is therefore important.

Halvorsen and Andresen⁴⁰ demonstrated that pH-stabilization efficiently reduced the corrosion rates in presence of large amounts of total Ac⁻ (up to 70000 ppm). By increasing the pH of the aqueous phase in the bottom of the line the concentration of HAc was reduced, and hence the partial pressure of HAc over the liquid. This caused a decrease in the concentration of HAc in the condensing liquid, and a reduction in the top-of-line corrosion rate. The tests were carried out in 60-80 wt-% ethylene glycol in water mixtures at 0 °C to 85 °C, under CO₂ partial pressures from 0.4 bar to 0.8 bar.

Gunaltun and Belghazi²⁶ demonstrated the feasibility of two alternative mitigation techniques for top-of-line corrosion in presence of acetic acid. One method was batch inhibition, and the other was pH-stabilization by means of an amine base.

Summary of corrosion studies

There seems to be an agreement that HAc can increase the cathodic reaction rate (hydrogen evolution reaction) if the concentration is significant. The corrosion rate can be correlated to the concentration of undissociated HAc present in the brine. Equilibrium calculations involving all species and reactions in the system are therefore essential to understand test results and predict the corrosiveness in the field from formation water analyses. The three main cathodic reactions appear to be:



where the rate of reaction (3) is limited by the preceding slow hydration of CO₂:³²⁻³⁴



Equations (1)-(3) reflect overall reaction, and do not purport to indicate detailed mechanisms of the proton reduction. The relative contribution from each of these reactions routes depends on the concentrations, temperature, pH, convection, etc. The H₂ evolution from HAc seems to be under activation control.

It also seems established that HAc or Ac⁻ may inhibit the anodic part reaction, in particular at room temperature.

The laboratory data shows some apparent discrepancies with respect to corrosion rates in the presence of HAc and CO₂. A weak inhibitor effect of HAc on general corrosion was observed at room temperature. At higher temperatures HAc caused increased corrosion rates. The experimental results of the present project indicate that the difference in temperature and the type of attack are the key parameters to understand the different observations.

One item of confusion is frequently encountered in the literature on the effect of HAc, namely that HAc is a stronger acid than carbonic acid. The source of this confusion is that the term “carbonic acid” is often also used to denote a solution of dissolved CO₂ (carbonated water). In order to contribute to clear this confusion, the basics of aqueous CO₂ chemistry are recapitulated.⁵¹⁻⁵² CO₂ gas dissolves readily in water and forms dissolved CO_{2(aq)}. The dissolved CO₂ reacts with H₂O to form carbonic acid, H₂CO₃.



The H₂CO₃ concentration is only a small fraction (ca. 1/600) of the CO_{2(aq)} concentration. H₂CO₃ dissociates to form bicarbonate, HCO₃⁻.



The dissociation constant K_a of H₂CO₃ according to Eq. (6), expressed as pK_a, is 3.5 at 25 °C, i.e. lower than for HAc (pK_a 4.8). Accordingly, H₂CO₃, which is the cathodic reactant in CO₂ corrosion,³²⁻³⁴ is a stronger acid than HAc. Equations (5) and (6) can be added to give Eq. (7).

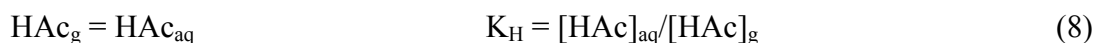


The apparent pK_a of dissolved CO₂ according to the reaction in Eq. (7) is ca. 6.3, which is the commonly listed value in textbooks. The reason for the frequent use of this quantity is that it is easily and precisely determined and applied from CO₂ analysis and pH measurements, while the pK_a of H₂CO₃ can only be determined from kinetic measurements with relatively poor precision.⁵¹

Physio-chemical data for HAc

Diffusion coefficients. Garsany et al. determined the diffusion coefficient for HAc^{30, 33} from limiting current measurements. The results were D = 1.0·10⁻⁹ m²/s at 25 °C, and 2.3·10⁻⁹ m²/s at 60 °C.

Solubility of HAc gas in water. Johnson and co-workers⁴¹ and Khan and co-workers⁴² have recently reported Henry's constants (K_H) for the equilibrium:



The two sets of data are in mutual agreement (within 20 %). Using Johnson's data⁴¹ the constant equals 4.1·10³ M/atm at 25 °C. The reaction is exothermic, ΔH = -52 kJ/mole. K_H at other temperatures can be estimated using the Van t'Hoff isochore (dlnK/dT = -ΔH/(RT²)),⁴³ see Table 1.

The results show that HAc gas is strongly soluble in water. The equilibrium partial pressure of HAc (P_{HAc}) over 1 mM (60 ppm) HAc solution is less than 1 Pa at temperatures up to about 100 °C. The gas phase is accordingly not a big reservoir for HAc. The HAc in the water phase can therefore mostly be treated as a closed system (no supply from the gas phase), contrary to the case of CO₂, where a large reservoir exists in the gas phase.

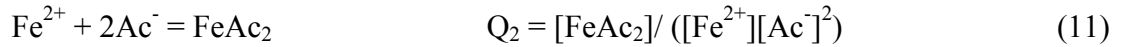
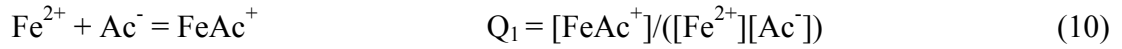
Partitioning of HAc between oil and water. Reinsel and co-workers⁴⁴ reported the oil-water partitioning coefficient

$$K_{o/w} = [\text{HAc}]_{\text{oil}} / ([\text{HAc}] + [\text{Ac}^-])_{\text{aq}} \quad (9)$$

of HAc in two different crude oils. The partitioning coefficients were calculated from analysis of the residual concentration of total Ac^- in the aqueous phase. The dissociation of HAc in the aqueous phase was not taken into consideration. This explains to large extent the pH dependence of the reported partitioning coefficients. A fraction of 1-2 % of the HAc was present in the oil phase at pH 4. These data indicate that the oil can serve as a reservoir for HAc, at least at low water cuts.

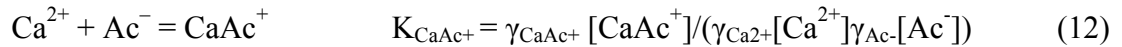
Borgund and Barth⁴⁵ also measured the partitioning of HAc between a mixture of crude oil plus n-pentane (4:1) and water. pH was not varied in this study. The results, indicate that HAc is partitioned essentially 100 % to the water phase. The resolution of the graphs does not allow calculation of the oil-water partitioning coefficient, but the magnitude appears at least not to be higher than those reported in Ref. 44.

Acetate complexes of Fe^{2+} and Ca^{2+} . Palmer and Hyde⁴⁶ report conditional formation constants (Q) for the two ferrous acetate complexes:



The paper gives data for $\log Q_1$ and $\log Q_2$ as functions of temperature (50-300 °C) and ionic strength. The magnitude of the formation constants increases with increasing temperature; selected values are given in Table 2.

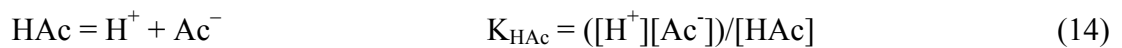
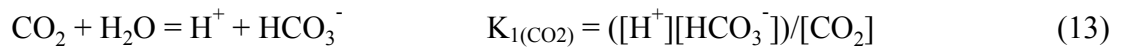
Seewald and Seyfird⁴⁷ reported the formation constant (K_{CaAc^+}) for the CaAc^+ complex, see Table 3.



where the γ 's denotes activity coefficient of the species indicated by the subscripts. These values are slightly higher than the corresponding values for FeAc^+ at zero ionic strength.⁴⁶ In formation waters with high content of calcium, a significant fraction of Ac^- should therefore be present as CaAc^+ .

EQUILIBRIUM CALCULATIONS

The following calculations are included to illustrate the behavior of the two buffer systems involved when both CO_2 and HAc are present. The calculations apply to condensed water conditions in the bottom of the line. The ratio of weak acids to their conjugate bases is given as a function of pH:



The two equilibria are linked through the common ion, H^+ .

In the buffer region we neglect the self-dissociation of the acids, and a weak acid HA is converted to the conjugate base A⁻ by the overall corrosion reaction:



Thus, before the onset of FeCO₃ precipitation we have in a system with CO₂ and HAc:

$$[\text{Fe}^{2+}] = ([\text{Ac}^{-}] + [\text{HCO}_3^{-}]) / 2 \quad (16)$$

For the CO₂ system, we can assume that the gas phase contains sufficient CO₂ to always keep the level of CO₂ in the (bulk) water phase constant (open system). The solubility of HAc is so high in the aqueous phase that essentially all HAc is present in the water phase, and cannot be replenished from the gas phase (i.e. a closed system). Exceptions from this may be in the first stages of condensation in a gas well or pipeline, or in an oil system with low water cut. Furthermore, transport of HAc from the water in the bottom of a pipe to the condensing water at the top of the pipe will occur through the gas phase. For the CO₂ system we therefore assume:

$$[\text{CO}_2] = \text{constant} \quad (17)$$

[HCO₃⁻] is given by equations (13) and (16). For the HAc we have (in condensed water):

$$[\text{HAc}] = [\text{HAc}]^0 - [\text{Ac}^{-}] \quad (18)$$

where [HAc]⁰ is the initial concentration of HAc.

For a given pH we can calculate the concentrations of the bases from Eqs. (13)-(14), using Equations (17)-(18) for the acid concentrations. The corresponding Fe²⁺ concentration is then given by Eq. (16). The results of such calculation are plotted as pH vs. [Fe²⁺] in Figure 1 for both of the test conditions; 25 °C with 1 bar CO₂, and 80 °C with 0.5 bar CO₂ (0.1-0.3 wt-% NaCl). The equilibrium constants in Table 4 were taken from Refs. 48-49:

Also included in Figure 1 are curves for a system with only CO₂ (no HAc), a system with constant HAc concentration (open system), and the saturation line for FeCO₃. It can be seen that the closed HAc system approaches the system with only CO₂ with increasing pH. CO₂/HCO₃⁻ is then the dominating buffer system. At lower pH the HAc/Ac⁻ buffer system is dominating. The change in concentration of the species vs. pH in a system with 600 ppm is shown in Figures 1c-d.

Formation of ferrous acetate complexes was not included in the calculations in Figure 1. A calculation example relevant to the present test conditions is shown in Figure 2 (80 °C, 0.5 bar CO₂, 600 ppm (10 mM) HAc added from start, with the increase in [Fe²⁺] and pH caused solely by corrosion, ref. Fig. 1). With 600 ppm HAc initially, less than 12 % of the Fe(II) is present as FeAc⁺ at pH 6. The formation of the di-acetate complex is negligible under these conditions. Also included in Fig. 2 is a calculation with 6000 ppm (100 mM) HAc initially. In this case, nearly 60 % of the Fe(II) is present as acetate complexes at pH 6. The di-acetate concentration is no longer negligible, but is not included in the calculation. This calculation shows that complex formation is not very important under the test conditions covered in this report, since the HAc concentration was limited to 600 ppm. However, the

acetate complexes can be significant at higher temperature and higher pH, with more Ac^- and/or iron, and should therefore be included in equilibrium calculations under such conditions. Furthermore, the complex formation shifts the $\text{HAc} = \text{Ac}^- + \text{H}^+$ equilibrium towards the right hand side (i.e. decreases pH), and lowers the concentration of free Fe^{2+} . The conditions for iron carbonate formation thus become less favorable. This should be taken into account in corrosion tests involving corrosion product films at elevated temperatures.

EXPERIMENTAL METHOD

Test solutions were prepared from distilled water, analytical grade HAc and reagent grade NaCl. The Fe^{2+} rich replenishment solutions were prepared by corroding commercially available steel wool in the brine under 1 bar CO_2 atmosphere at 50 °C. The steel wool was degreased in acetone prior to use.

The corrosion experiments were carried out on rotating cylinder specimens machined from X65 pipeline steel. Exception was one test with St52 grade steel, which is noted in the text and figures. The elemental analysis and microstructure of the steels used are given in Table 5. The test specimens were pre-treated by grinding with 1000 mesh SiC paper wetted with isopropanol, and degreasing in acetone.

Corrosion was studied electrochemically by use of a commercially available potentiostat equipped with an eight-channel multiplexer. A three-electrode configuration was used in all the measurements. The counter electrode was an AISI 316 stainless steel ring placed inside the cell, surrounding the specimen. The tip of a carbon steel wire was used as reference electrode for the potentiostat, in order to avoid potentiostat stability problems connected to high impedance reference electrodes and low conductivity solution. The wire was insulated by a PTFE hose; only the end of the wire was exposed to the solution. The tip was located 3-5 mm from the working electrode.

Corrosion rates were determined from linear polarization resistance (LPR),⁵⁵ using a 0.1 mV/s potential scan from -5 to +5 mV vs. the corrosion potential. The interval between the LPR measurements was in most cases 60 minutes. The parameters used for electrochemical measurements and corrosion rate calculations are summarized in Table 2. A data logger was used to monitor the corrosion potential of the specimen vs. the Ag/AgCl (3 M KCl) reference half-cell of the combination pH electrode. The cell temperature and the solution pH were also recorded by this logger. The logging frequency was synchronized with the potentiostat, logging the corrosion potential a few minutes before the LPR scan. Potentiodynamic scans were performed at the end of the test. All the reported results were corrected for electrolyte resistance determined by electrochemical impedance spectroscopy.

Pit depths were measured by optical microscopy. The depth of the deepest pit was used to calculate the time averaged pit penetration rate for the duration of the test. Metal loss was determined by mass loss measurements and iron counts in some tests. Iron(II) concentration was determined by spectrophotometry at 508 nm as ortho-phenanthroline complex. The mass loss corrosion rate was calculated as the area and time averaged penetration rate for the duration of the test. The mass loss was also used to determine the constant (B) used for calculation of the corrosion current from LPR,⁵⁶⁻⁵⁷ since the complexity of the part reactions complicates calculation from Tafel slopes. B-values of about 20 mV were determined, in agreement with experience from CO_2 corrosion.⁵⁷⁻⁵⁸

A schematic drawing of the test set-up is shown in Figure 3. A peristaltic pump brought the test solution from the reservoir (a 25-litres HDPE tank) to the test cell. The flow rate was 0.5-1 liter/h. A

magnetic stirrer was used to keep the solution properly mixed in the test cell. An overflow pipe maintained a constant liquid volume in the cell. The liquid discharged from the cell was collected in a drain tank. The reservoir tank and the test cell were continuously purged with CO₂. Water-cooled reflux condensers were mounted at the gas outlets of the reservoir and test cell in order to minimize loss of water and HAc. The discharge gas and liquid were passed through water locks to avoid air ingress. The temperature was regulated by a heating plate fitted with a temperature sensor in the cell. An enclosure was built around the rotating cylinder electrode motor. This enclosure was purged with dry CO₂ gas to minimize ingress of water vapor to the bearings and contacts.

Test procedure. The test solution was prepared in the 25 liters reservoir tank. The accuracy of the concentrations was within 2 % relative error. The content of residual HAc in the discharged test solution was checked in some tests. The HAc concentration was determined by acid-base titration* of the water collected in the drain tank. The results confirmed that no significant amount of HAc had escaped from the cell via the gas phase. This finding is reasonable, considering the low vapor pressure of HAc over aqueous solutions.

The test solutions that were saturated in FeCO₃ were prepared by the following procedure. The Fe²⁺ concentration at the FeCO₃ saturation point was calculated using thermodynamic data, see Table 4. The stoichiometric amount of steel wool was then added to the test solution in the reservoir barrel and allowed to corrode overnight under CO₂ atmosphere before use. This corrosion reaction corresponds to adding FeCO₃ (Fe + CO₂ + H₂O = FeCO₃ + H₂). The Fe²⁺ concentration was then checked by chemical analysis. A small amount of solid FeCO₃ was added in the test cell. This procedure ensured that the solution was saturated or slightly supersaturated. The pH and Fe²⁺ measured in the test cell corresponded closely to the pre-calculated value.

RESULTS AND DISCUSSION

The present experimental work with low Fe²⁺ concentrations focused on gas condensate pipeline conditions. Furthermore, it was selected to focus on bottom of line corrosion. Low Fe²⁺ concentration here means concentrations below or equal to FeCO₃ saturation (rather than supersaturated). Four cases were investigated:

1. High temperature (80 °C) / low Fe²⁺ (pipeline inlet conditions).
2. Low temperature (25 °C) / low Fe²⁺ (inlet of carbon steel pipe after cooling in corrosion resistant alloy piping).
3. Low temperature (25 °C) / FeCO₃ saturated (pipeline outlet).
4. High temperature (80 °C) / FeCO₃ saturated (intermediate condition where ferrous carbonate film is stable and likely to be present).

The rotation rate was kept constant at 1900 RPM, unless otherwise noted. This corresponds to a peripheral velocity of 1 m/s of the cylinder specimen. In terms of mass transfer, this rotation rate

* The test solution was purged with N₂ to remove residual CO₂. The solution was titrated with 0.001 M or 0.01 M NaOH using pH-metric end point determination. The amount of acetic acid determined by titration corresponded to 100 ± 5 % of the added amount, when corrected for the Fe²⁺ concentration (which gives the amount of acetic acid converted to acetate).

corresponds to 1.5 m/s flow velocity in a 25 mm ID pipe at 25 °C, and 1.2 m/s at 80 °C. The wall shear stresses are 6 and 3 Pa, respectively.

Initial tests were performed with in 0.1 wt-% NaCl under gas condensate conditions. With the high corrosion rates encountered in some of the tests, the solution resistance constituted a significant fraction of the total resistance measured by LPR. The NaCl concentration was therefore raised to 0.3 %, since 0.1 % gave problems in the first tests. Some of the corrosion rate vs. time curves appear rather noisy. Some fluctuations in the corrosion rate may be expected on a specimen undergoing localized corrosion. Furthermore, the current distribution and potential distribution around pits are non-uniform. The reference electrode will accordingly sense a periodic disturbance in potential each time a pit rotates past the tip of the reference electrode.

Case 1: 25 °C, low Fe²⁺: With no HAC present the final corrosion rate was ca. 4 mm/y (Fig. 4). The corrosion potential was -0.67 V. The corrosion attack was uniform. No significant amounts of corrosion film were observed.

Tests were carried out with 60 ppm, 200 ppm, and 600 ppm added HAC (corresponding to 1 mM, 3.33 mM, and 10 mM, respectively). As an example, the detailed results of the tests with 200 ppm added HAC are shown in Figure 5. The maximum Fe²⁺-concentration during the test was 1.6 ppm (0.03 mM). This means that about 2 % of the HAC was converted to Ac⁻. The average mass loss corrosion rate was ca. 1.5 mm/y, i.e. lower than in the pure CO₂ system. The LPR corrosion rate was about 4-5 mm/y in the start of the test, but decreased to about 0.5 mm/y after half a day. After one day of exposure the LPR corrosion rate started to increase again, and the rate appeared to stabilize around 1.5-2 mm/y after 5 days of exposure. Few, but very deep pits were observed on the surface of the exposed specimens (Fig. 5c). The specimen was also attacked in the crevice between the specimen and the PTFE of the specimen holder. The maximum (time average) penetration rate of the pits was ca. 10 mm/y. The corrosion potential was as high as -0.60 V at the beginning of the test. The potential dropped after 0.5 days, but fluctuated thereafter between -.62 and -0.60 V. The test at 200 ppm was repeated with an St52 specimen (detailed results not shown). The average corrosion rate was slightly higher than with the X65 specimen. Some pits were found at the surface; with maximum pit penetration rates of 7 mm/y. Larger areas of the surface had corroded uniformly, compared to the X65 specimen. The corrosion potential was high also on the St52 specimen, -0.59 V.

Figure 6 compares the polarization curves for 200 ppm HAC with the HAC free solution. The curves were measured at the end of the tests in Fig.5 and Fig. 4, respectively. The HAC clearly shifted the anodic Tafel curves to higher potentials, i.e. a sign of anodic inhibition. The cathodic current density increased with addition of HAC. Although the cathodic polarization curves show no Tafel Behaviour, a corrosion current of about 1-3 A/m² can be estimated with 200 ppm HAC, in agreement with the mass loss rate. At high cathodic polarization the current densities approached the calculated^{34,50} diffusion limiting current for 200 ppm HAC, as indicated by the dashed line. However, in general the cathodic curves did not show clear limiting current plateaus.

Pitting corrosion attacks were observed in all the tests in the range 60-600 ppm added HAC. Figure 7 shows the appearance of a specimen exposed in a brine with 600 ppm HAC. Repeated tests with no electrochemical measurement on the specimens showed similar pitting attacks. It was therefore concluded that the pits were not provoked by the electrochemical measurements.

Case 2: 80 °C, low Fe²⁺. At 80 °C the baseline corrosion rate was about 10 mm/y in the absence of HAc. Figure 8 shows the results from a test with 200 ppm added HAc. The maximum Fe²⁺-concentration was 11 ppm (0.2 mM), so no more than about 10% of the added HAc was converted to Ac⁻. The average mass loss corrosion rate was 24 mm/y. The LPR corrosion rate was about the same value. The corrosion attack was uniform. The specimen exposed at 200 ppm was partly covered with a 20 micrometer thick corrosion film. The film cracked upon drying and was not adherent. The film had a high fraction of voids. The corrosion rate increased with increasing HAc in the range 60 ppm to 200 ppm.

In these tests at 80 °C the corrosion potential increased with increasing HAc concentration to about -0.59 V at 600 ppm HAc. The anodic polarization curve was shifted to higher potentials with increasing HAc concentration, indicating anodic inhibition (as in the tests at 25 °C). The corrosion attack was uniform in all the tests with 60-600 ppm HAc at 80 °C.

FeCO₃ saturated solution (Case 3 and Case 4). A few tests were performed with FeCO₃ saturated solutions (Case 3 and Case 4). Some corrosion film was observed by optical microscopy after the test at 25 °C. A few pits were observed after stripping the film with inhibited HCl. After the tests at 80 °C, a 20-40 micron thick corrosion film covered most of the rotated specimen whereas some parts of the surface had no film. The film cracked upon drying and did not adhere well to the steel surface. None of the films offered significant protection against corrosion.

Corrosion rates vs. HAc concentration

Figure 9 shows the corrosion rates of all the tests plotted as function of the concentration of undissociated HAc (calculated from [HAc]⁰ and [Fe²⁺]). At 25 °C, the mass loss and LPR corrosion rates reached a maximum at 60 ppm HAc. Above this value these average rates decreased to a level of 2-3 mm/y. The corrosion potential increased to about -0.6 V. The maximum pit penetration rates, however, were much higher than the average rates, and they increased with the HAc concentration to about 30 mm/y at 600 ppm HAc. The trend of the LPR corrosion rate in Figure 9 resembles closely the one reported in Ref. 6.

At 80 °C, the average corrosion rates increased steadily with increasing HAc concentration. The corrosion attack was uniform. The corrosion potential increased with increasing HAc concentration from ca. -0.7 V at 0 ppm to -0.6 V at 600 ppm.

The data from the FeCO₃ saturated solutions are also plotted in Figure 9. The average corrosion rates seem to follow the trend of the solutions with low Fe²⁺ level, despite some variations in the amount of corrosion film formed on the test specimens. The films were accordingly poorly protective.

The present test results with low Fe²⁺ concentration seem to rationalize and unify many of the results reported in the literature on the effect of HAc. The effect of temperature and the type of attack seems to be the key issue. At room temperature the HAc inhibited general corrosion, and reduced the average corrosion rates. However, deep pits developed. The number of pits was low. This resembles the pitting behavior of some passive metals, where the nucleation of a few pits can depolarize the electrode to a potential below the pit nucleation potential. The existing pits continue to grow, thus causing attacks with few, but deep pits. The corrosion potential increased with increasing HAc concentration. This shift was caused by the inhibition of the anodic part reaction (the anodic polarization curve was shifted to higher potentials) and an increase in the cathodic reaction rates. Both of these factors contribute to a high risk of localized corrosion in spots where the inhibition effect fails.

The tendency of localized corrosion attack may depend on the type of steel tested (ref. the difference between X65 and St52). However, the data are yet too few to suggest any trends.

At 80 °C the average corrosion rates were much higher, and the attack uniform. HAc caused a shift of the anodic polarization curves to higher potentials, as it did at 25 °C, indicating inhibition of the anodic part reaction. However, this inhibition evidently did not reduce the general corrosion rates at this temperature.

The tests results show that no protective (macroscopic) corrosion film needs to be involved to get localized attack in the presence of HAc at lower temperatures. However, in cases with high temperature and high potential corrosivity, the effect of HAc on the corrosion film properties may be an important issue.

The test results at 80 °C indicated that the corrosion was dependent on flow. The polarization curves did in most cases show no clear limiting current plateau in the vicinity of the corrosion potential. A limiting current for HAc was only observed at high cathodic polarization. The diffusion limited current of HAc reduction is plotted as a function of HAc concentration in Figure 10. The limiting current on bare electrodes are higher than the actual corrosion rates above 60 ppm HAc. Since some corrosion film was observed at the specimens at 80 °C, the actual diffusion limit may be lower than the theoretical one. The corrosion caused by HAc is probably under activation control. The contributions from H⁺ and H₂CO₃ may be under full or partial mass transfer control. The reaction-limited currents for H₂CO₃ reduction are ca. 1.5 and 6 mm/y at 25 and 80 °C, respectively.³⁴ The diffusion-limited current for reduction of free protons in the bulk solution is also included in Figure 10. These results show that HAc is the dominating cathodic reactant above ca. 60 ppm (1 mM) HAc (with ca. 1 bar CO₂), in agreement with field experience⁹⁻¹⁰ and laboratory data.³²⁻³³ The relative effect of a given HAc concentration will decrease with increasing CO₂ pressure. This is in line with the cited field experience,⁹⁻¹⁰ since the adverse effect of HAc was observed at low CO₂ partial pressures, whereas at high CO₂ pressures the corrosion rates always were unacceptably high, even in wells without HAc.

Solution chemistry effects

Figure 11 shows mass loss corrosion rates as a function of NaCl concentration in brine with 200 ppm HAc added, and partial pressure of 0.5 bar CO₂. These short-term tests (< 6 hrs.) tests were performed at 80 °C. The pH was lower than the steady value in the long-term tests, e.g. Fig. 8. The average corrosion rates are therefore somewhat higher, just as in the early stage of Fig. 8. The corrosion rates increased with NaCl concentration from around 40 mm/y below 0.1 wt-% NaCl to nearly 70 mm/y above 1 wt-% NaCl. The polarization curves in Fig. 11, measured at 0.3 % and 3 %, show that the increase was caused by increase of both the cathodic and the anodic current. The increased cathodic rates can be explained from the solution chemistry. Due to the decreasing activities with increasing salt content, the pK_a of HAc decreases from 4.85 in 0 % NaCl to 4.47 in 3 % NaCl.⁴⁹ This 0.4 units drop gives rise to a pH drop of about 0.2 pH-units ($\text{pH} \approx \frac{1}{2} (\text{pK}_a - \log[\text{HAc}])$). Mass transfer calculations show that a change from pH 3.7 to pH 3.5 causes a rise in the diffusion limited H⁺ reduction current of more than 10 mm/y. The cathodic polarization curves in Fig. 11 indicate ca. 20 mm/y increase. The increased cathodic rates may tentatively be correlated to lifting of the anodic inhibition with increasing chloride content. This example illustrates the importance of detailed speciation of the solution, and the fact that solution equilibrium H⁺ can contribute significantly to the worst case corrosion rate in the lower range of pH encountered in oilfield systems, as pointed out by several other workers.^{19, 33} The results furthermore

indicate that the 0.1-0.3 wt-% NaCl brine used in the present work represents condensed water fairly well.

Figure 12a shows mass loss corrosion rates as a function of total Ca^{2+} concentration in brine with 200 ppm HAc added, and partial pressure of 0.5 bar CO_2 . The pH was adjusted to pH 4.6 in all of these tests. This intermediate pH was chosen to avoid CaCO_3 precipitation, while keeping the influence of H^+ to a low level. The corrosion rate decreased significantly from 0 ppm to 300 ppm Ca^{2+} . Above this value, however, the corrosion rate reached a steady rate of ca. 30 mm/y. The polarization curves (Fig. 12b) show that the cathodic current decreased with increasing Ca^{2+} concentration from 0 ppm to 110 ppm. From 110 ppm to 1080 ppm only a minor change occurred. The reduced cathodic current is consistent with reduced HAc concentration. No deposits were observed at the electrode surface, so CaCO_3 scaling is not a probable explanation for the reduced current. Fig. 12c shows the calculated HAc concentration plotted as a function of total Ca^{2+} concentration. The change was calculated considering the formation of CaAc^+ complex according to Eq. (12). Consumption of Ac^- by the complex formation causes further dissociation of HAc to replace the Ac^- bound as complex, ref. Eq. (14). The calculated HAc concentration decreases continuously, and shows a 20% reduction at ca. 1500 ppm Ca^{2+} . Several factors may contribute to this discrepancy between experiment and calculation. The Ca^{2+} may form significant amounts of other complexes, e.g. CaCl^+ and $\text{Ca}(\text{OH})^+$. These complexes were not considered in Fig. 12. The reduction in HAc concentration might therefore not be as large as calculated according to Eq. (12). The results may contribute to explain the different results observed between 3% NaCl brine and synthetic formation brine in the work of George et al.¹⁹ The complex formation constants increase with increasing temperature, and complex formation should therefore be considered in work with formation waters at high temperature. This also applies to Fe^{2+} complex formation in the evaluation of FeCO_3 film formation experiments in presence of HAc and Ac^- at high temperatures.

SUMMARY AND CONCLUSIONS

The literature on CO_2 corrosion in presence of HAc was reviewed. Some studies reported increased corrosivity in presence of HAc, whereas others reported that HAc works as an inhibitor. Most of the corrosion data reported in the literature was, however, found to be consistent when the effect of temperature and type of attack observed in the present work was taken into consideration. Literature data indicated that HAc corrosion could be mitigated by means of corrosion inhibitors. The physiochemical properties of HAc was also reviewed: diffusion coefficient, partial pressure of HAc over aqueous HAc solutions, HAc solubility in oil, and formation constants of ferrous and calcium acetate complexes.

The corrosion behavior of X65 pipeline steel in solutions containing CO_2 , HAc and 0.1-0.3 % NaCl was investigated on rotating cylinder specimens in glass cells. The initial concentration of HAc was varied between 0 and 600 ppm (0-10 mM). The test solutions were continuously replenished. The Fe^{2+} concentration was in most of the tests held far below the FeCO_3 saturation limit. The electrode rotation rate was 1900 RPM, corresponding to ca. 1 m/s peripheral velocity. The corrosion rates were measured electrochemically and by mass loss measurements.

The experimental results were summarized in Figure 9. The results show that:

- At 25 °C the corrosion attack was localized. The pit penetration rate increased with increasing HAc concentration to about 30 mm/y at 600 ppm HAc. The average (mass loss) corrosion rate

decreased with increasing HAc concentration above 60 ppm, due to inhibition of the anodic reaction. The baseline CO₂ corrosion rate with no HAc present was 4 mm/y.

- At 80 °C the average corrosion rate increased with increasing HAc concentration, reaching 45 mm/y at 600 ppm HAc. The corrosion attack was uniform. The baseline CO₂ corrosion rate with no HAc present was 10 mm/y.
- The anodic part reaction was inhibited by HAc, both at 25 and 80 °C. This was evident from the fact that the anodic polarization curves were shifted to higher potentials with increasing HAc concentration. The results indicated that the anodic inhibition effect at 80 °C was reduced with increasing salt content.
- Corrosion films were formed at the surface of the corroding specimens at 80 °C, and in the saturated solutions at 25 °C. The films were poorly protective (at the time-scale of the tests).
- Long term tests and proper inspection of the specimens after testing are essential to identify any localized corrosion attack, in particular at lower temperatures where the anodic inhibition phenomenon leads to reduced general corrosion rates in presence of HAc. This is also essential in inhibitor test in presence of HAc.³⁷
- The corrosion rate depended on rotation rate. The flow dependence was not investigated in detail, but the data indicate that the flow dependence may mainly be related to the reduction of H⁺ and H₂CO₃, while reduction of HAc was activation controlled.
- It is essential to determine the concentrations of the involved reactants and products by equilibrium calculations to understand corrosion test results in presence of CO₂ and HAc. Depending on the concentrations, temperature, and convection all of the species H⁺, H₂CO₃ and HAc may play a significant role as cathodic reactants.
- Addition of Ca²⁺ ions to the test brine reduced the corrosion rate significantly (at constant pH). The preliminary results indicate that this reduction was caused by CaAc⁺ complex formation leading to reduced concentration of HAc.
- Formation of acetate complexes of Fe²⁺ and Ca²⁺ should be considered at high temperatures. The FeAc⁺ complex may reduce the driving force for protective FeCO₃ film formation. The pH and HAc calculations may be biased in formation waters with high content of Ca²⁺ if CaAc⁺ complex formation is not taken into account. Field specific corrosion and inhibition tests should therefore be carried out in brines that closely resemble the actual composition of the formation water.

In summary, a number of factors appear to determine the corrosion rate in presence of HAc and CO₂. These factors include:

- Concentration of the reactants and products
- Electrochemical kinetics of cathodic reactions (activation control or mass transfer control)
- Electrochemical kinetics of the anodic reaction (inhibition by HAc, localized or uniform dissolution)
- Corrosion product films (kinetics of formation and morphology)

While significant progress has been made in the understanding of the three first bullet points, it appears that further work is needed to obtain reliable corrosion predictions in systems with HAC present. Little work has yet been done on the behavior of corrosion product films in such systems, and this topic should be emphasized in further work.

ACKNOWLEDGEMENT

The main part of the present work was carried out within IFE's Joint Industry Project "Kjeller Acetic Acid Project" (1999-2002). The project was funded by BP, ENI Agip, Hydro, Shell, Statoil, and TotalFinaElf. The authors acknowledge the funding, and the technical advice from the steering committee during the project. Additional work on the effect of NaCl and Ca²⁺ was funded by IFE.

REFERENCES

1. B.Hedges, D.Paisley, R.Woolham, "The Corrosion Inhibitor Availability Model", CORROSION/2000, paper no. 34, (Houston, TX: NACE International, 2000).
2. S.D.Kapusta, B.F.M.Pots, R.A.Connel, "Corrosion Management of Wet Gas Pipelines", CORROSION/99, paper no. 45, (Houston, TX: NACE International, 1999).
3. I.Rippon, "Carbon Steel Pipeline Corrosion Engineering: Life Cycle Approach", CORROSION/2001, paper no. 55, (Houston, TX: NACE International, 2001).
4. M.-R.Bonis, J.-L.Crolet, "An Inhibition Policy Based on Laboratory and Field Experience", CORROSION/98, paper no. 103, (Houston, TX: NACE International, 1998).
5. NORSOK Standard M-001 Materials Selection, rev. 4, Aug. 2005. Standards Norway (www.standard.no).
6. J.-L-Crolet, N. Thevenot, A. Dugstad, "Role of Free Acetic Acid on the CO₂ Corrosion of Steels", CORROSION/99, Paper no. 24, (Houston, TX: NACE International, 1999).
7. J.A.Dougherty, "A Review of the Effect of Organic Acids on the CO₂ Corrosion", CORROSION/2004, Paper no. 376, (Houston, TX: NACE International, 2004).
8. J.-L. Crolet, M.R. Bonis, "The Role of Acetate in CO₂ Corrosion", CORROSION/83, Paper no. 160, (Houston, TX: NACE International, 1983).
9. M.R. Bonis, J.-L. Crolet, "Basics of the Prediction of the Risk of CO₂ Corrosion in Oil and Gas Wells", CORROSION/89, Paper no. 466, (Houston, TX: NACE International, 1989).
10. J.-L. Crolet, M.R. Bonis, "Prediction of the Risk of CO₂ Corrosion in Oil and Gas Wells", 22nd Offshore Technology Conference, Houston, TX, 1990.
11. M.B. Kermani, A. Morshed, Corrosion, 59, 659 (2003).
12. J.-L. Crolet, M.R. Bonis, "Why So Low Free Acetic Acid Thresholds in Sweet Corrosion at Low P(CO₂)", CORROSION/2005, Paper no. 272, (Houston, TX: NACE International, 2005).
13. B. Hedges, L. McVeigh, "The Role of Acetate in CO₂ Corrosion - The Double Whammy", CORROSION/99, Paper no. 21, (Houston, TX: NACE International, 1999).
14. M. Ueda, H. Takabe, "Effect of Organic Acid on CO₂ Corrosion of Carbon and Cr Bearing Steels", CORROSION/98, Paper no. 35, (Houston, TX: NACE International, 1998).

15. S. Tebbal, N. Hackermann, "Effect of Buffer Capacity on the CO₂ Pitting of Steel", CORROSION/99, Paper no. 23, Houston, TX: NACE International, 1999).
16. S. Tebbal, N. Hackermann, Corros. Sci., 34, 1787 (1993).
17. A. Dugstad, H. Hemmer, H. Kooyman, W. Wilhelmsen, "Kjeller Sweet Corrosion III – Final report", IFE report no. IFE/KR/F-93/091, Institute for Energy Technology, (1993) (Restricted).
18. Y. Sun, K. George, S. Nestic, "The Effect of Acetic Acid on Localized CO₂ Corrosion in Wet Gas Flow", CORROSION/2003, Paper no. 327, Houston, TX: NACE International, 2003).
19. K. George, S. Nestic, C. de Waard, "Electrochemical Investigation and Modelling of Carbon Dioxide Corrosion of Carbon Steel in the Presence of Acetic Acid", CORROSION/2004, Paper no. 379, Houston, TX: NACE International, 2004).
20. S. Wang, K. George, S. Nestic, "High Pressure and Corrosion Electrochemistry and the Effect of Acetic Acid", CORROSION/2004, Paper no. 375, Houston, TX: NACE International, 2004).
21. K. George, S. Wang, S. Nestic, K. de Waard, "Modelling of CO₂ Corrosion of Mild Steel at High Pressures of CO₂ and in the Presence of Acetic Acid", CORROSION/2004, Paper no. 623, Houston, TX: NACE International, 2004).
22. M. Singer, S. Nestic, Y. Gunaltun, "Top of the Line Corrosion in Presence of Acetic acid and Carbon Dioxide", CORROSION/2004, Paper no. 377, Houston, TX: NACE International, 2004).
23. C. Méndez, M. Singer, A. Camacho, S. Hernández, S. Nestic, "Effect of Acetic Acid, pH and MEG on the CO₂ Top of the Line Corrosion", CORROSION/2005, Paper no. 278, Houston, TX: NACE International, 2005).
24. O.A. Nafday, S. Nestic, "Iron Carbonate Scale Formation and CO₂ Corrosion in the Presence of Acetic Acid", CORROSION/2005, Paper no. 295, Houston, TX: NACE International, 2005).
25. Y.M. Gunaltun, D. Larrey, "Correlation of Cases of Top of Line Corrosion With Calculated Water Condensation Rates", CORROSION/2000, Paper no. 71, Houston, TX: NACE International, 2000).
26. TY.M. Gunaltun, A. Belghazi, "Control of Top of Line Corrosion by Chemical Treatment", CORROSION/2001, Paper no. 33, Houston, TX: NACE International, 2001).
27. X.P.Guo, Z.Y. Chen, D. Liu, K. Bando, Y. Tomoe, "The Effect of Acetic Acid and Acetate on CO₂ Corrosion of Carbon Steel", CORROSION/2005, Paper no. 306, Houston, TX: NACE International, 2005).
28. T. Hurlen, S. Gunvaldsen, F. Blaker, "Effects of Buffers on Hydrogen Evolution at Iron Electrodes" Electrochim. Acta, 29, 1163 (1984).
29. G. Bech-Nielsen, "The Anodic Dissolution of Iron – V", Electrochim. Acta, 19, 821 (1974).
30. Y. Garsany, D. Pletcher, B. Hedges, "Speciation and electrochemistry of brines containing acetate ion and carbon dioxide", J. Electroanal. Chemistry, 538-539, p. 285 (2002).
31. Y. Garsany, D. Pletcher, B. Hedges, "The Role of Acetate in CO₂ Corrosion of Carbon Steel: Has the Chemistry Been Forgotten?", CORROSION/2002, Paper no. 273, Houston, TX: NACE International, 2002).
32. Y. Garsany, D. Pletcher, B. Hedges, "The Role of Acetate in CO₂ Corrosion of Carbon Steel: Studies Related to Oilfield Conditions", CORROSION/2003, Paper no. 324, Houston, TX: NACE International, 2003).

33. Y. Garsany, D. Pletcher, D. Sidorin, W.M. Hedges, *Corrosion*, 60, 1155 (2004).
34. S. Nestic, J. Postlethwaite, S. Olsen: "An electrochemical model for prediction of corrosion of mild steel in aqueous carbon dioxide solutions", *Corrosion*, 52, 280 (1996).
35. D. Abayarathna and A. Naraghi, "Inhibition of CO₂ Corrosion of Carbon Steel in the Presence of Acetate", CORROSION/2002, Paper no. 291, Houston, TX: NACE International, 2002).
36. M.W. Joosten, J. Kolts, J.W. Hembre, "Organic Acid Corrosion in Oil and Gas Production", CORROSION/2002, Paper no. 294, Houston, TX: NACE International, 2002).
37. M.W. Joosten, G.D. Harris, R.L. Hudgins, D. A. Daniels, K.M. Cloke, "Localized Corrosion Resulting from Inhibition in Oil and Gas Production Environments Containing Acetate", CORROSION/2005, Paper no. 114, Houston, TX: NACE International, 2003).
38. N. Bretherton, R. Smith, G. Keilty, S. Ubbels, "Naphtenate Control: Is Acetic Acid Injection the Answer", 2nd Int. Symposium on Oilfield Corrosion, Paper no. SPE 95115, Society of Petroleum Engineers, Richardson, TX (2005).
39. R.L. Martin, P.D. Logan, "Laboratory and Field Study of the Influence of Simple Carboxylates on Oilfield Corrosion and Inhibition", 2nd Int. Symposium on Oilfield Corrosion, Paper no. SPE 95092, Society of Petroleum Engineers, Richardson, TX (2005).
40. A.M.K. Halvorsen, T.R. Andersen, "pH Stabilization for Internal Corrosion Protection of Pipeline Carrying Wet Gas With CO₂ and Acetic Acid", CORROSION/2003, Paper no. 329, Houston, TX: NACE International, 2005).
41. B.J. Johnson, E.A. Betterton, D. Craig, "Henry's Law Coefficients of Formic and Acetic Acid", *J. Atmospheric. Chem.*, 24, 113 (1996).
42. I. Khan, P. Brimblecombe, S. Clegg, "Solubilities of Pyruvic Acid and the Lower (C1 – C6) Carboxylic Acids.", *J. Atmospheric Chem.*, 22, 285, (1995).
43. P.W. Atkins, "Physical Chemistry", 2nd Ed., Oxford University Press, Oxford (1982).
44. M.A. Reinsel, J.J. Borkowski, J.T. Sears, "Partitioning Coefficients for Acetic, Propionic, and Butyric Acids in a Crude Oil/Water System", *J. Chem. Eng. Data*, 39, 513, (1994).
45. A.E. Borgund, T. Barth, "Migration Behaviour of Petroleum-associated Short-chain Organic Acids", *Org. Geochem.*, 20, 1019 (1993).
46. D.A. Palmer, K.E. Hyde, "An experimental determination of ferrous chloride and acetate complexation in aqueous solutions to 300 °C", *Geochimica et Cosmochimica Acta*, 57, 1393 (1993).
47. J.S. Seewald, W.E. Seyfird, "Experimental determination of portlandite solubility in H₂O and acetate solutions at 100-350 °C and 500 bars", *Geochimica et Cosmochimica Acta*, 55, 659 (1991).
48. J.E. Oddo, M.B. Tomson, "The prediction of Scale and CO₂ Corrosion in Oil Field Systems", CORROSION/99, Paper no. 41, (Houston, TX: NACE International, 1999).
49. Institute for Energy Technology, In-house solubility calculation model, SOL18 (2001).
50. NACE Publication 5A195: State-of-the-Art Report on Controlled-Flow Laboratory Corrosion Tests, NACE International, Houston (1995).
51. D. Palmer, R. van Eldik, *Chem.Rev.*, 83, 651 (1983)

52. N.N. Greenwood, A. Earnshaw, "Chemistry of the elements", Pergamon Press, Oxford (UK) (1984), p. 329.
53. J.D.Garber, R.S.Perkins, V.R.Jangama, R.R.Alapati, "Calculation of Downhole pH and Deleta pH in the Presence of CO₂ and Organic Acids", CORROSION/96, Paper no. 176, (Houston, TX: NACE International, 1996).
54. J.D.Garber, V.R.Jangama, J.Willmon, "Calculation of Downhole pH and Delta pH in the Presence of CO₂ and Organic Acids", CORROSION/97, Paper no. 606, (Houston, TX: NACE International, 1997).
55. M. Stern, A.L. Geary, J. Electrochem. Soc., 104 (1957), p. 56.
56. A.C. Makrides, Corrosion, 29 (1973), p. 148.
57. E.Gulbrandsen, J.Kvarekvål, H.Miland, "Effect of Oxygen Contamination on Inhibition Studies in CO₂ Corrosion", Corrosion, 61, 1086 (2005).
58. S. Nestic, J. Postlethwaite, S. Olsen, Corrosion, 52 (1996), p. 280.
59. I.Grenthe, H.Wanner, E.Östhols, "Guidelines for the Extrapolation to Zero Ionic Strength", OECD Nuclear Energy Agency, Thermochemical Data Bank Project, Publication # TDB-2, Le Seine-St. Germain, France (2000). URL: <http://www.nea.fr/html/dbtdb/guidelines/tdb2.pdf>

Table 1. Henry's constant for HAc in water.⁴¹

Temperature (°C)	K _H (10 ³ M bar ⁻¹)	P _{HAc} over 1 mM HAc (bar)
25	4.1·10 ³	2.4·10 ⁻⁰⁷
60	8·10 ² *	1·10 ⁻⁰⁶
80	2·10 ² *	6·10 ⁻⁰⁶
110	4·10 ¹ *	3·10 ⁻⁰⁵

* Estimated

Table 2. Formation constants for ferrous acetate complexes in 0.3 wt-% NaCl.⁴⁶

Temperature (°C)	log(Q ₁) FeAc ⁺	log(Q ₂) FeAc ₂
50	1.0	1.5
100	1.3	2.0
150	1.6	2.5
300	2.9	5.4

Table 3. Complex formation constant for calcium acetate complex.⁴⁷

Temperature (°C)	log(K _{CaAc⁺})
25	1.2
100	1.9
150	2.5
300	3.7

Table 4. Equilibrium constants used in the calculations.⁴⁸⁻⁴⁹

Temperature/ °C	25	80
P (CO ₂) / bar	1.0	0.5
[CO ₂] / mM	33.3	6.2
pK _{1(CO2)}	6.25	6.23
pK _{2(CO2)}	10.08	9.87
pK _(HAe)	4.66	4.81
pK _{sp} (FeCO ₃)	10.08	11.08

Table 5. Element analysis (wt-%) for the carbon steel specimens. Microstructure: Ferrite-pearlite.

Steel*	C	Si	Mn	S	P	Cr	Ni	V	Mo	Cu	Al	Sn	Nb
St52 (#53)	0.13	0.38	1.29	0.008	0.015	0.07	0.09	0.035	0.01	0.34	0.05	0.015	
X65 (#57)	0.08	0.25	1.54	0.001	0.019	0.04	0.05	0.095	0.01	0.02	0.038	0.001	0.043

*) Internal IFE steel reference number.

Table 6. Parameters used for electrochemical measurements and calculations.

Test specimen - cylinder	10 mm Ø x 10 mm H, $S=3.1 \text{ cm}^2$
Linear Polarization Resistance (LPR) - R_p - sweep rate	Potential ramp -5 to +5 mV vs E_{cor} 0.1 mV/s
Electrochemical Impedance Spectroscopy (EIS)	$\pm 5 \text{ mV rms.}, 5 \text{ kHz} - 0.01 \text{ Hz}$
Potentiodynamic sweep -cathodic -anodic	0 to -0.3 V vs. E_{cor} , 0.1 mV/s 0 to +0.1 V vs. E_{cor} , 0.1 mV/s
Corrosion Current Density, I_{cor}	$I_{cor} = B/(R_p S)$ B=20 mV, or based on mass loss data
Corrosion Rate, v_{cor}	$v_{cor}(\text{mm/y}) = 1.16 I_{cor}(\text{Am}^{-2})$
Reference Electrode	Steel / Ag/AgCl (3 M KCl) $E = 0.194 \text{ V vs. } she$

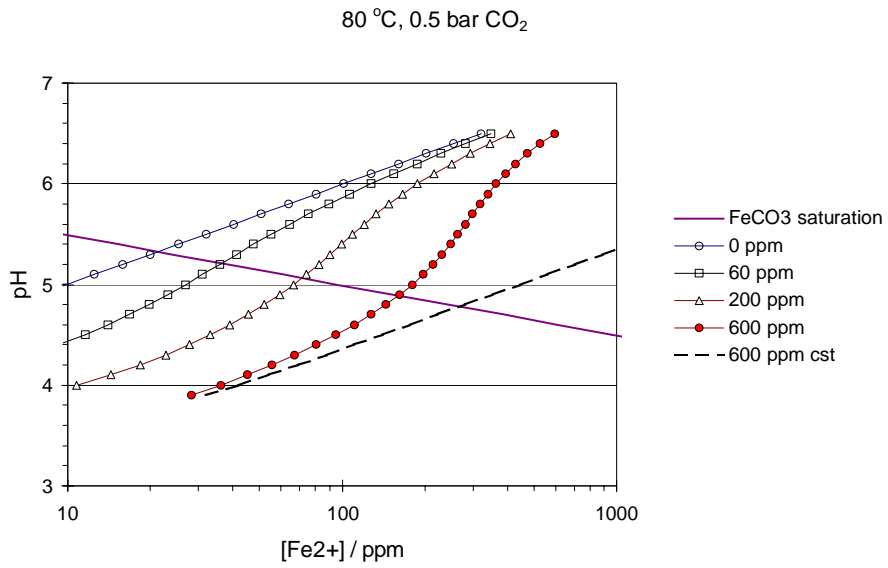
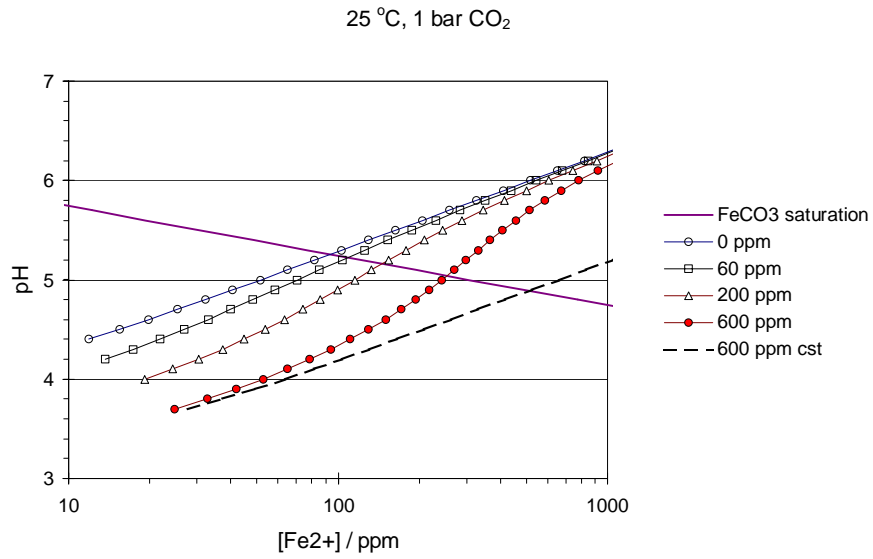


Figure 1a-b Caption overleaf.

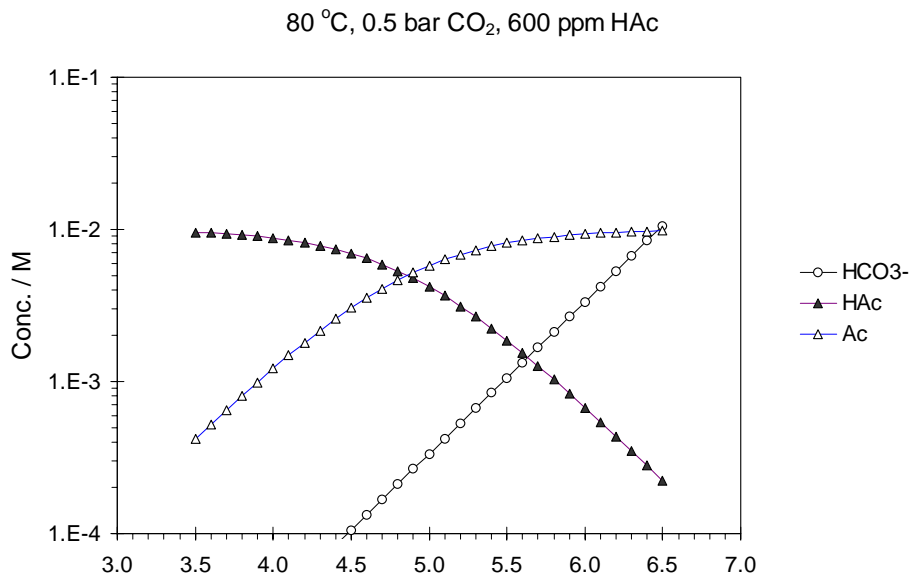
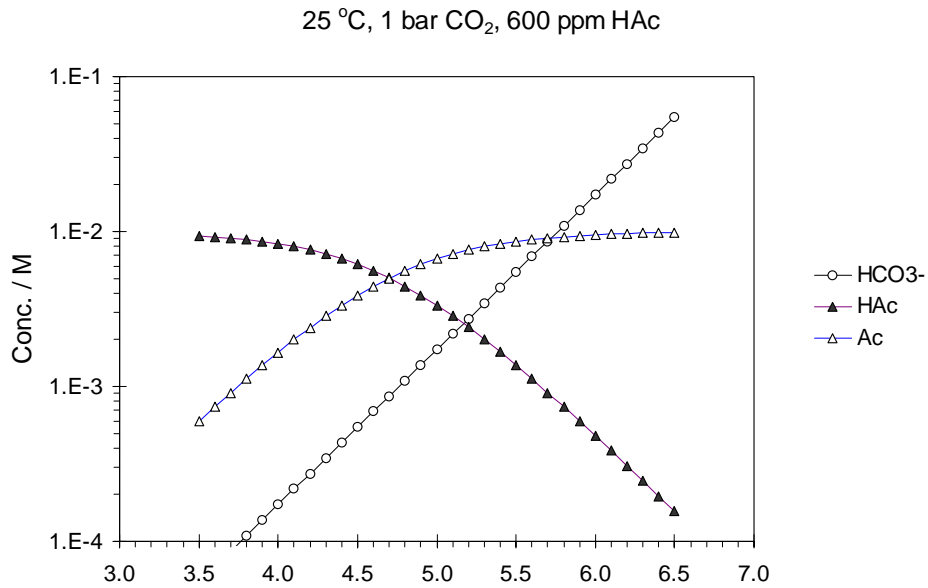


Figure 1 (a)-(b) Calculated pH vs. Fe²⁺ concentration for a corroding system with CO₂ and HAc present from the start and no replenishment of HAc. The concentrations in the legends refer to initial value of acetic acid ([HAc]⁰). Exceptions are the dashed curves which represent systems with [HAc]= 600 ppm constant. (c)-(d)-Distribution of species. Equilibrium constants from Refs. 48-49.

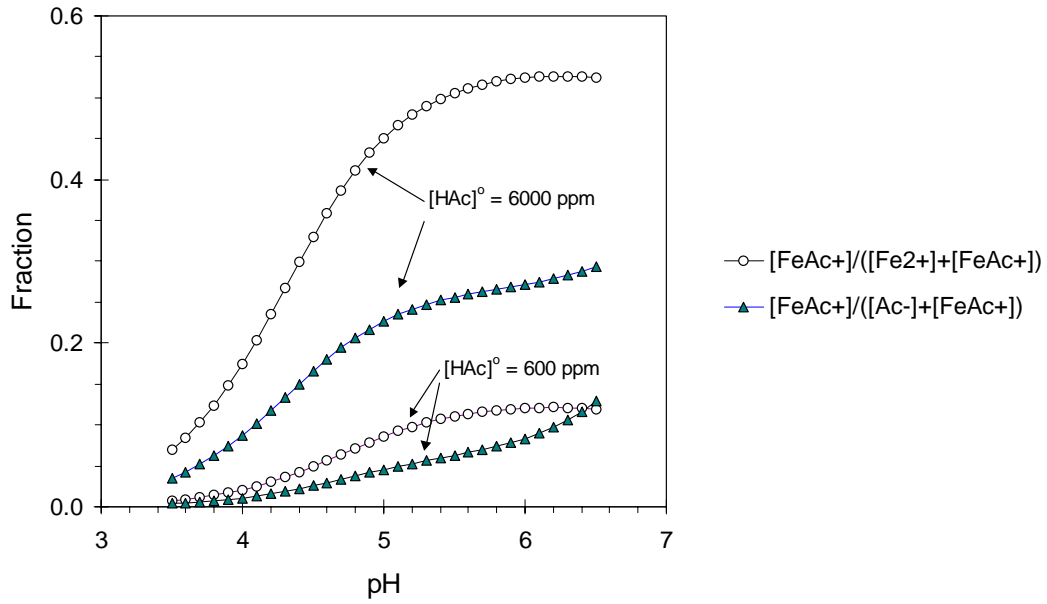


Figure 2 Concentration of FeAc^+ complex expressed as fraction of total Fe(II) and as fraction of total acetate ($\text{Ac}^- + \text{FeAc}^+$). 80°C , 0.5 bar CO_2 , $0.3\% \text{ NaCl}$. Condensing water conditions corresponding to the curves of Figs. 1b and 1d. Based on formation constants given in Ref. 46.

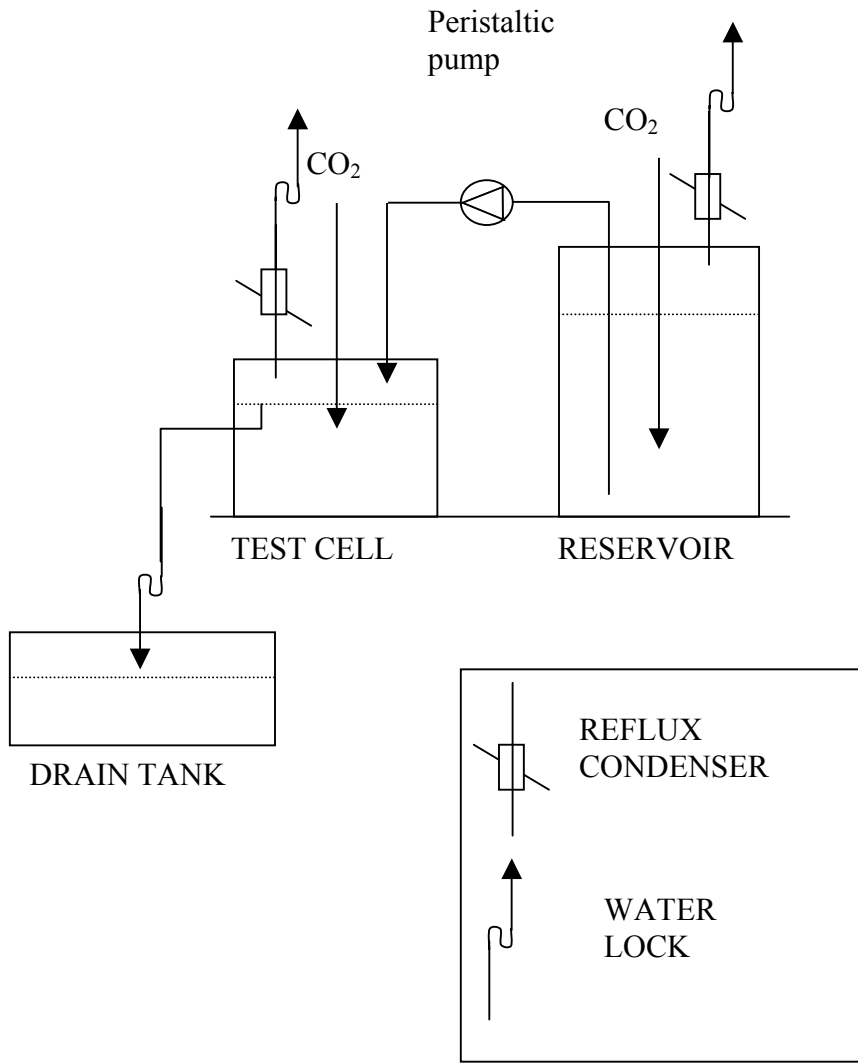
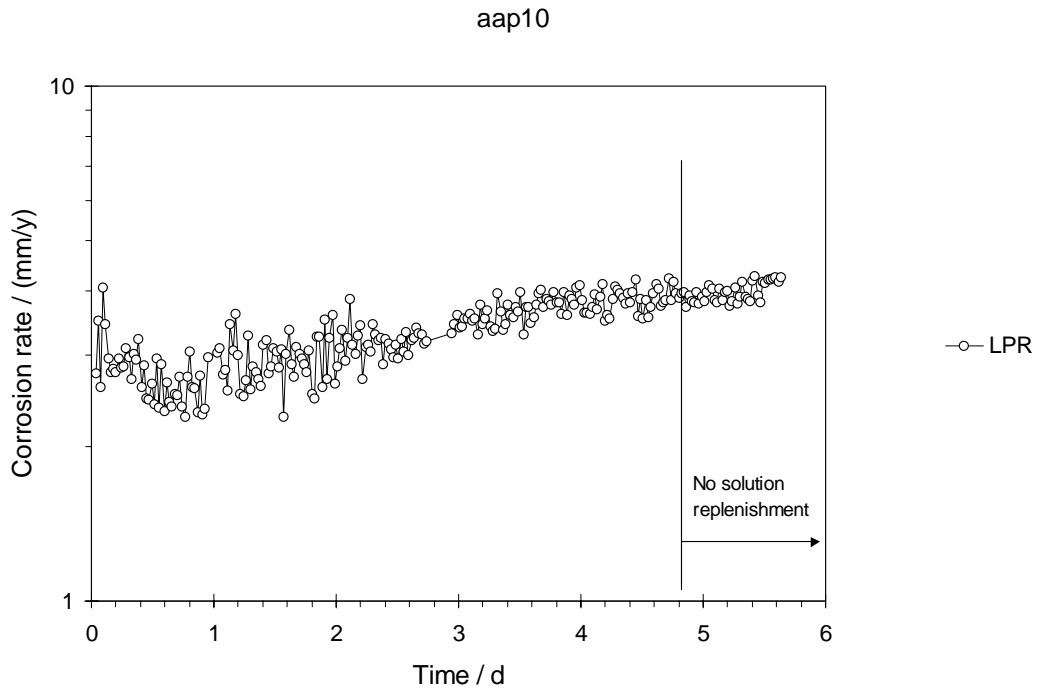


Figure 3 (a) Schematic of the test set-up in tests with rotating cylinder specimen.

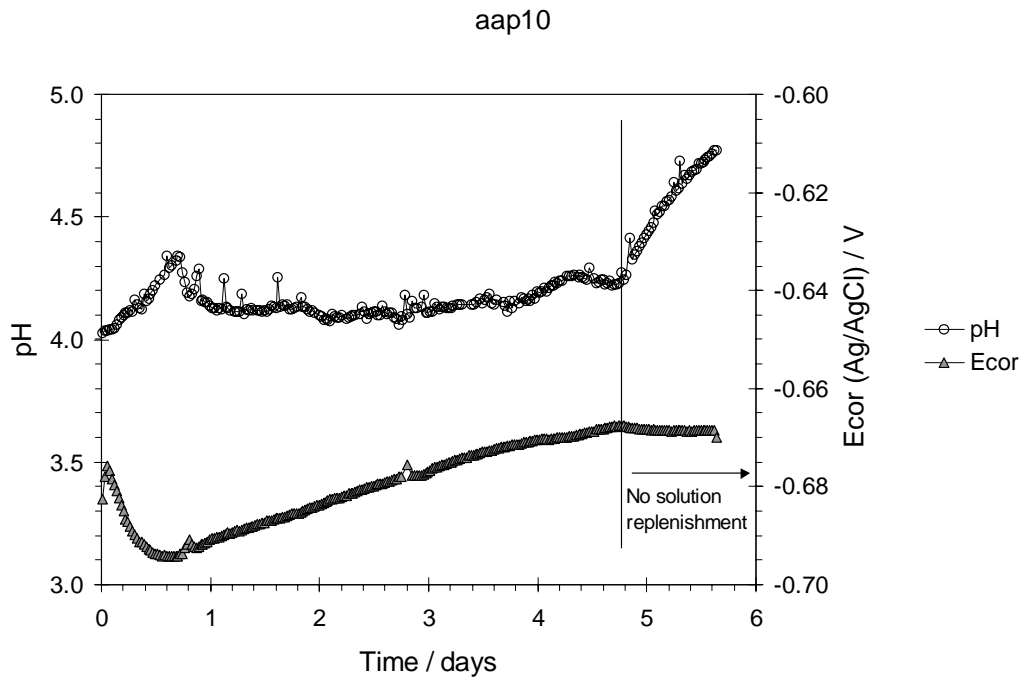
(Figure 4)

Temp. (°C)	[HAc] ⁰ (ppm)	P _{CO2} (bar)	Max [Fe ²⁺] (ppm)	[NaCl] (wt%)	RCE rotation (RPM)	B _{LPR} mV
25	0	1	6 (23)	0.1	1900	(20)

No solution replenishment last day of test, [Fe²⁺] increased to 23 ppm



(a)



(b)

Figure 4a-b Caption overleaf

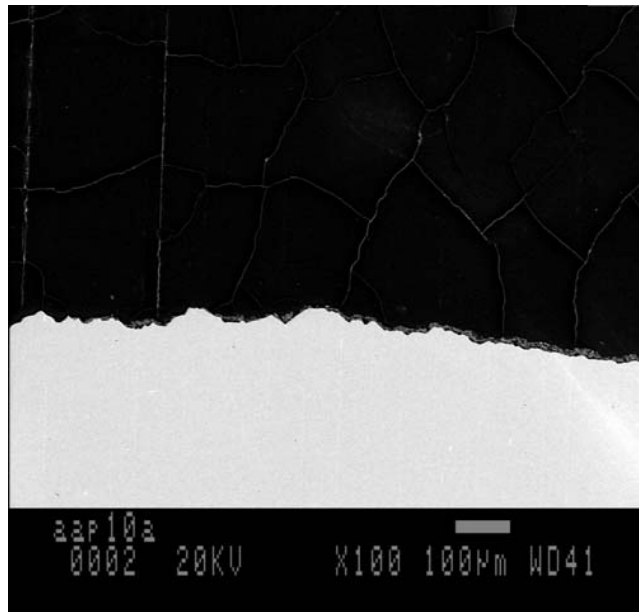


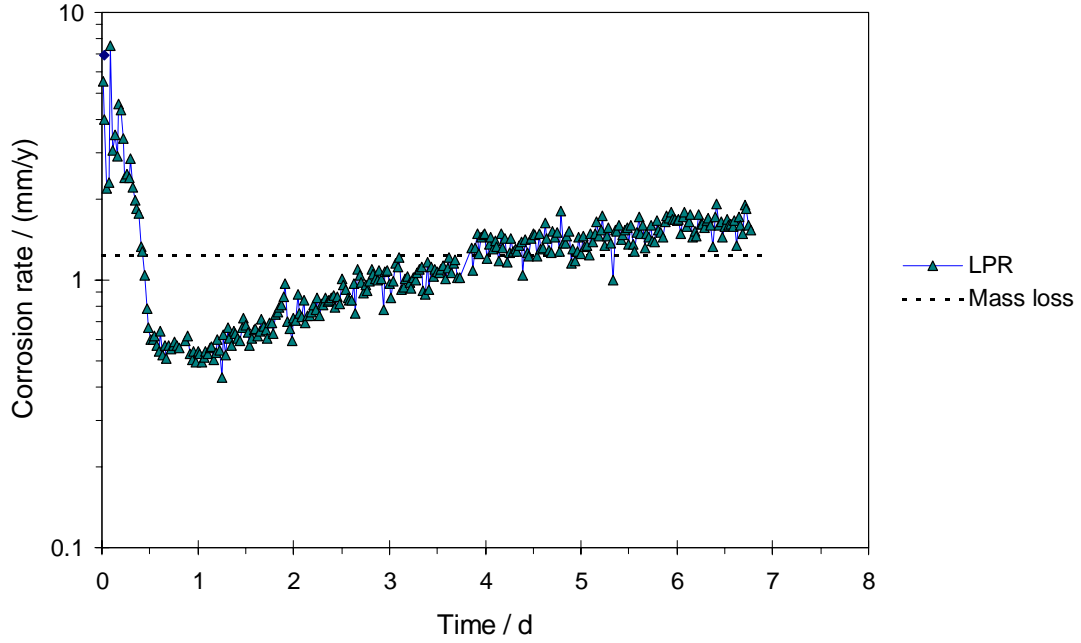
Figure 4 (a) Corrosion rate vs. time, (b) pH and E_{cor} , and (c) SEM image of test specimen cross-section. Test conditions, see Table on previous page.

(Figure 5)

Temp. (°C)	[HAc] ⁰ (ppm)	P _{CO2} (bar)	Max [Fe ²⁺] (ppm)	[NaCl] (wt%)	RCE rotation (RPM)	B _{LPR} mV
25	200	1	1.6	0.1	1900	26

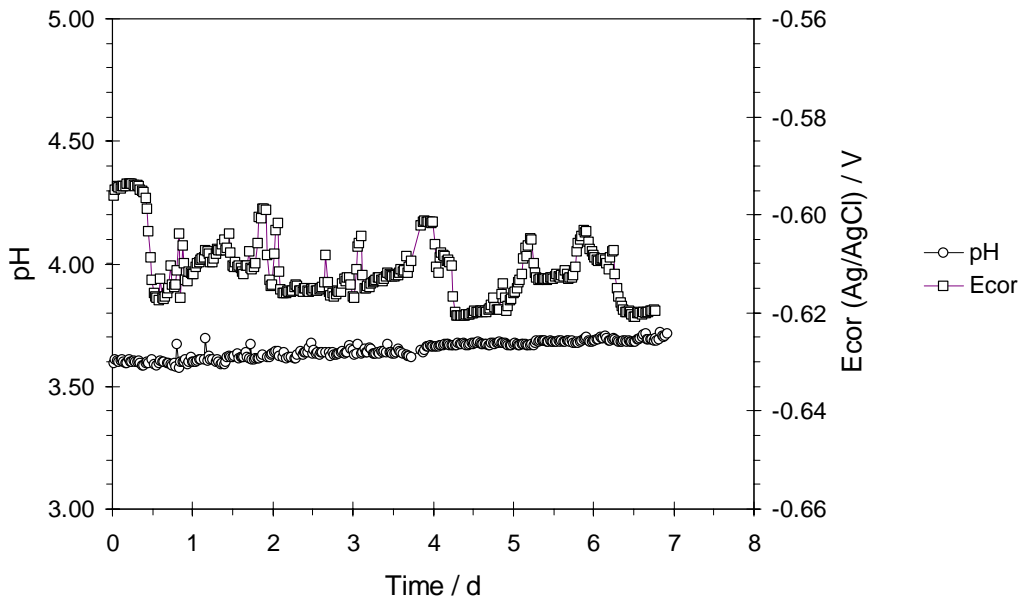
X65 steel

aap11



(a)

aap11



(b)

Figure 5a-b Captions overleaf

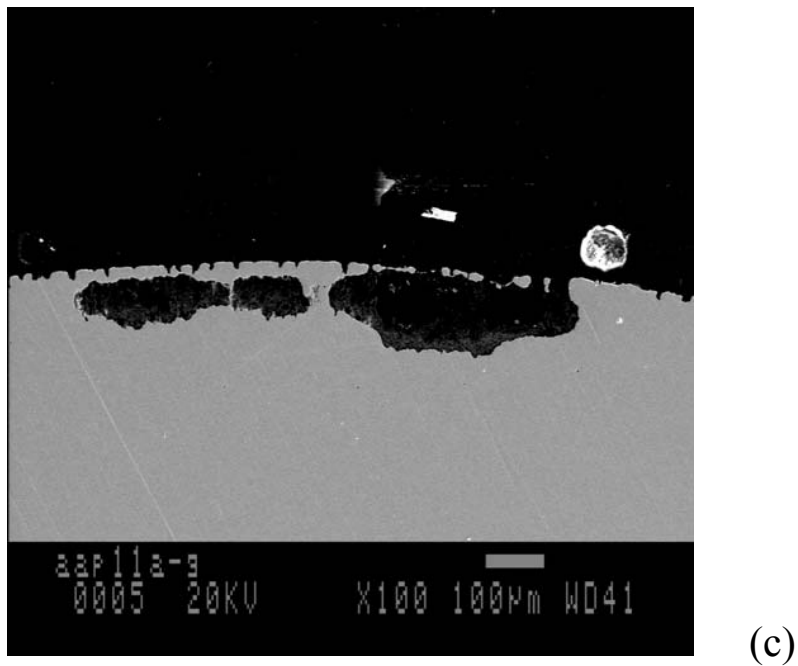


Figure 5 (a) Corrosion rate vs. time, (b) pH and E_{cor} , and (c) SEM image of test specimen cross section. Test conditions, see Table on previous page.

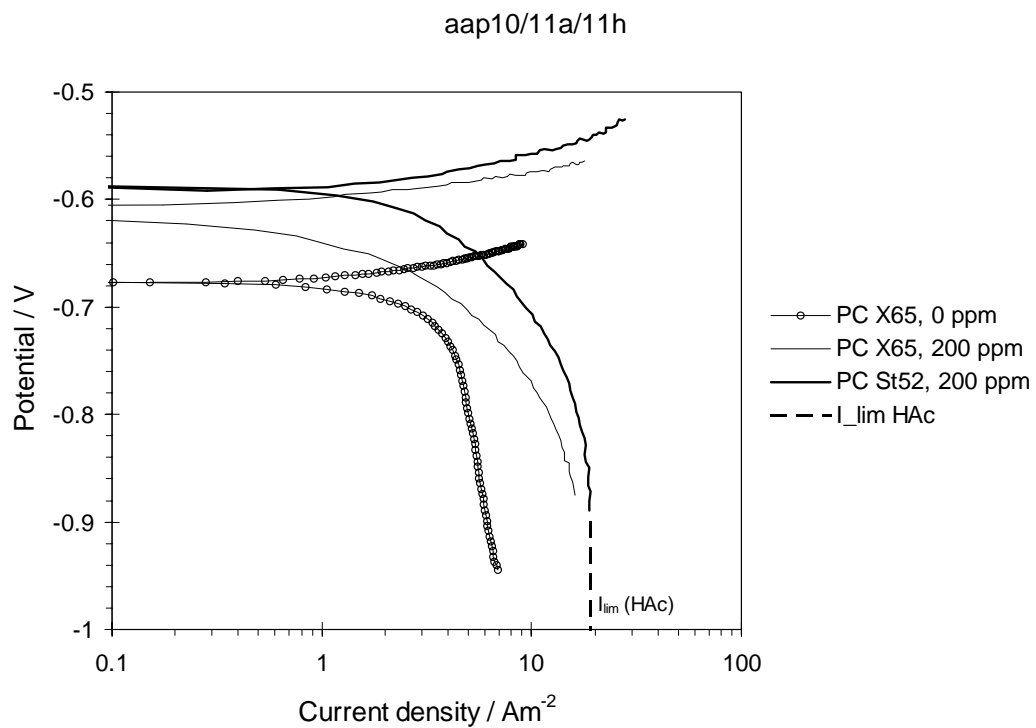


Figure 6 Polarization curves showing the effect of HAc on the part reactions (1 bar CO₂, 0.3 wt-% NaCl, 25 °C).

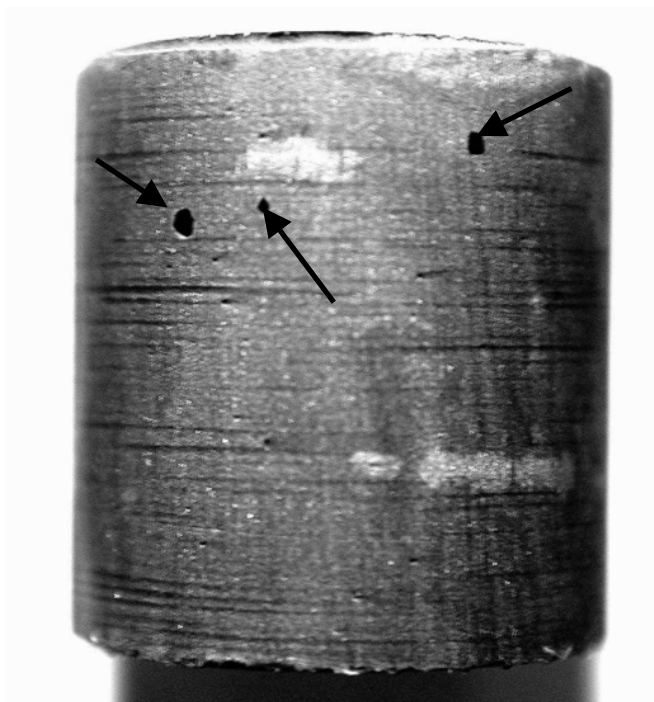
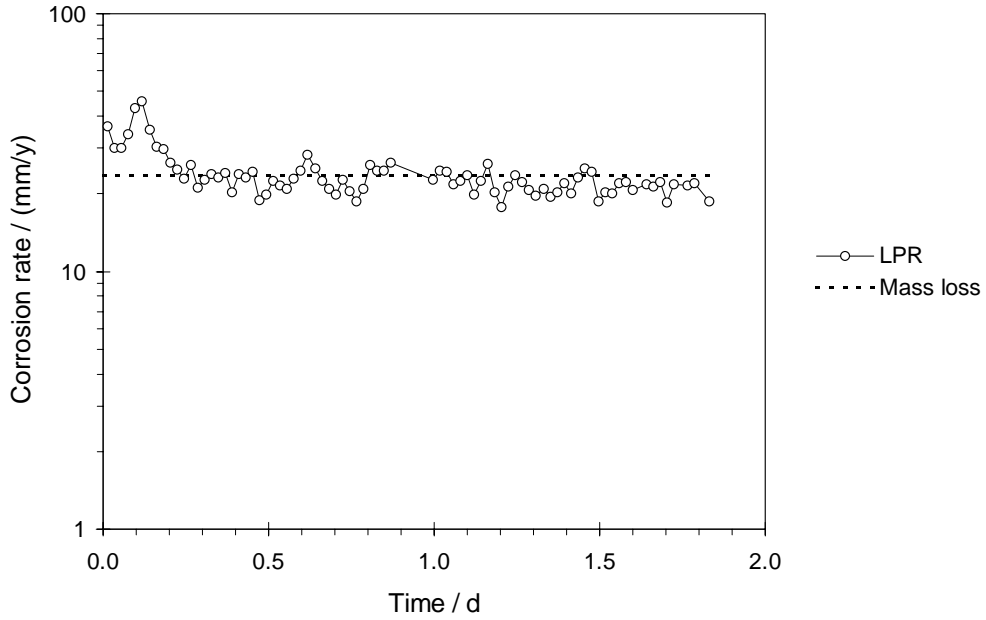


Figure 7 Deep pits (see arrows) on specimen exposed to 600 ppm HAc at 25 °C. (1 bar CO₂, 0.3 wt-% NaCl, < 1 ppm Fe²⁺)

(Figure 8)

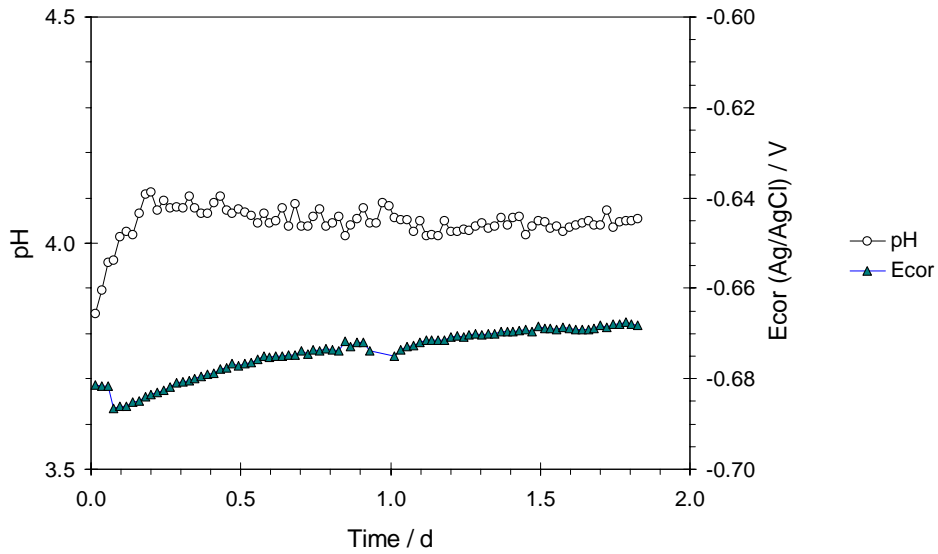
Temp. (°C)	[HAc] ⁰ (ppm)	P _{CO2} (bar)	Max [Fe ²⁺] (ppm)	[NaCl] (wt%)	RCE rotation (RPM)	B _{LPR} mV
80	200	0.5	11	0.1	1900	20

aap14



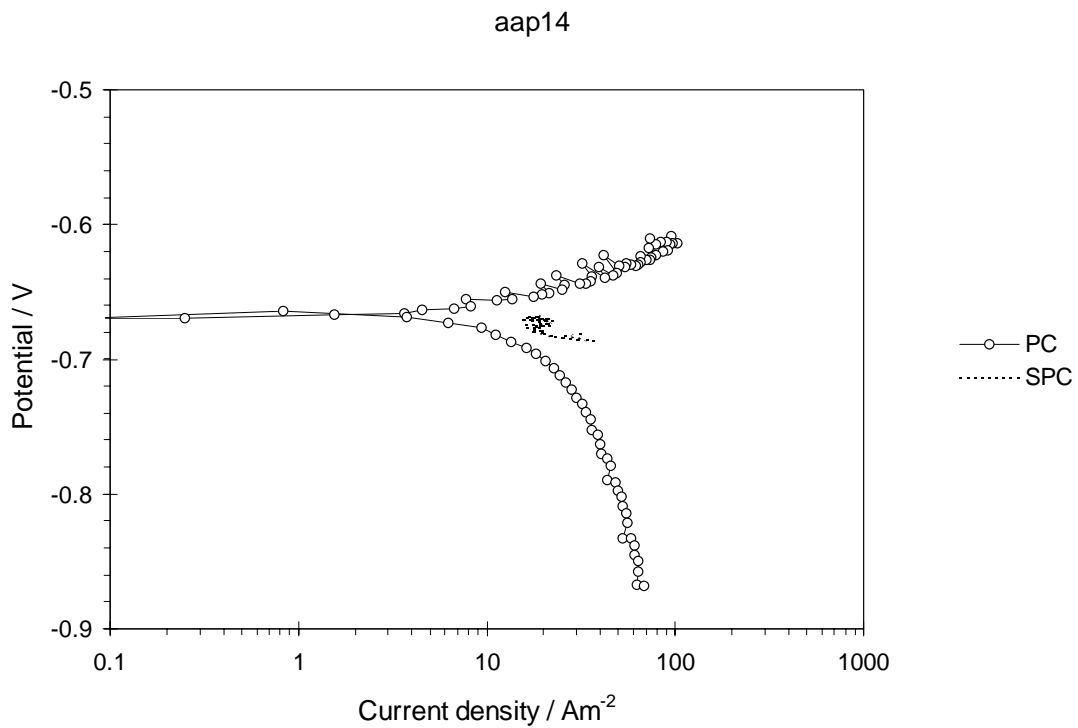
(a)

aap14

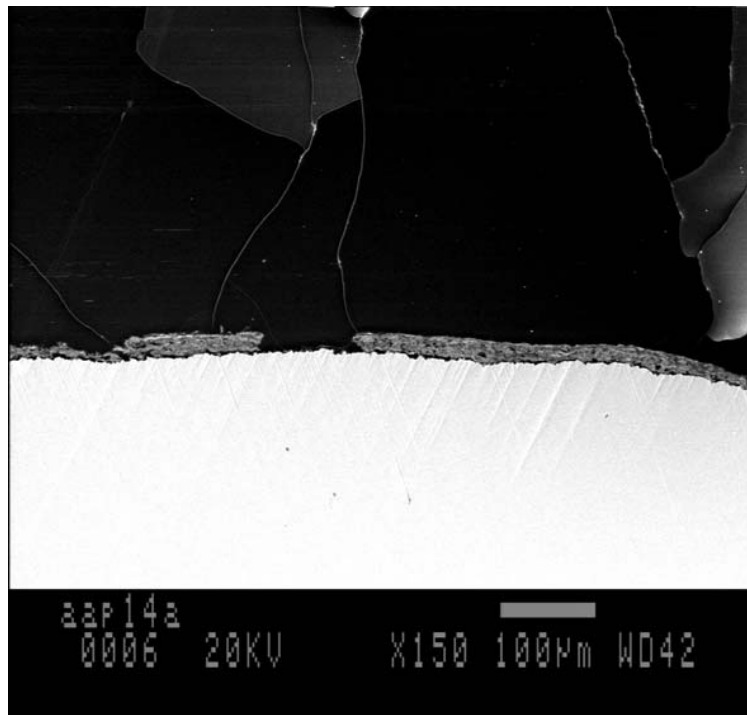


(b)

Figure 8a-b Captions overleaf



(c)



(d)

Figure 8 (a) Corrosion rate vs. time, (b) pH and E_{cor} , (c) Polarization curve (PC), (d) SEM image of specimen cross section. Test conditions, see table on previous page.

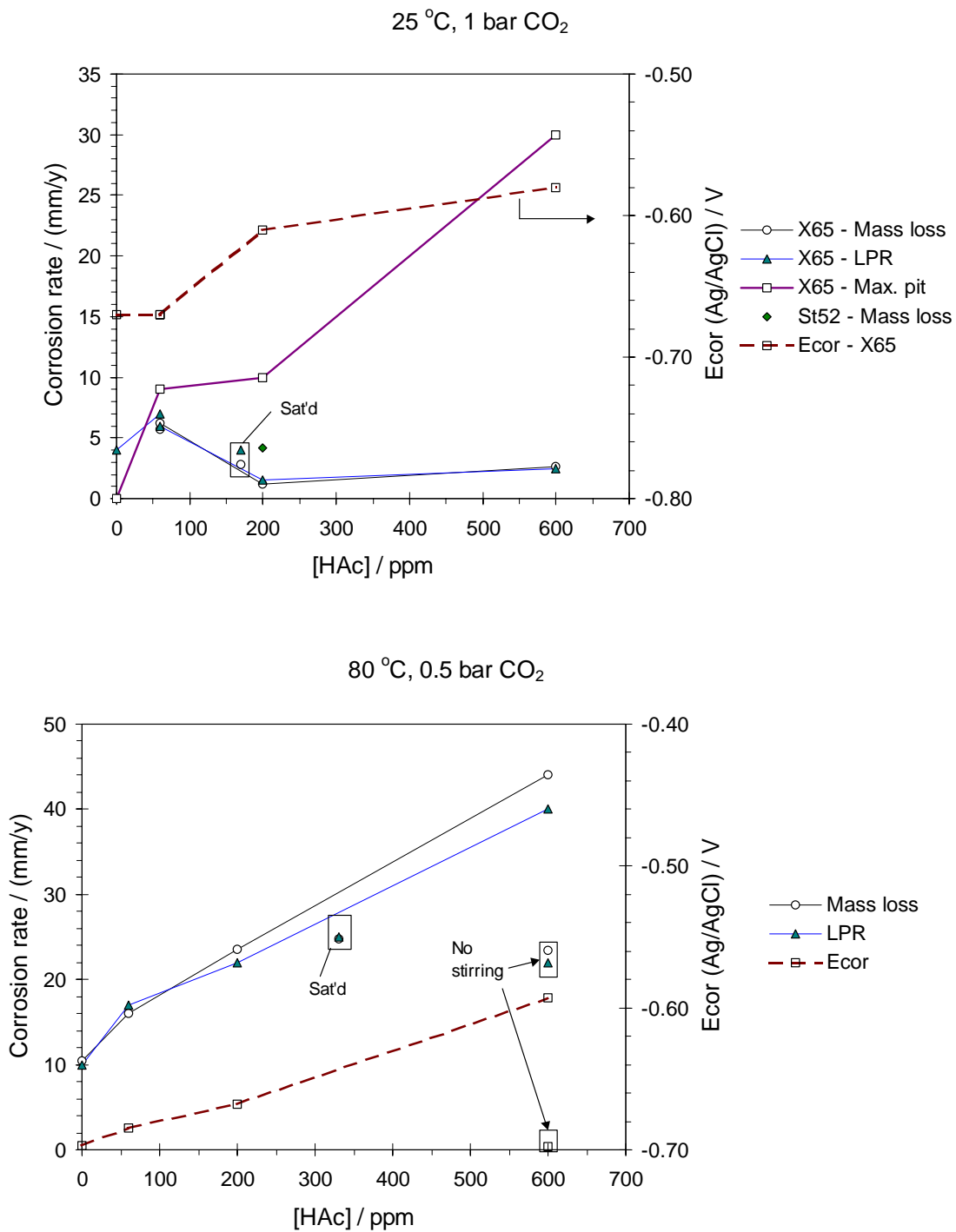


Figure 9 Corrosion rate vs. concentration of undissociated acetic acid at 25 °C with 1 bar CO₂ (top), and 80 °C with 0.5 bar CO₂ (bottom). The Fe²⁺ concentration was below 10-22 ppm. Exceptions are data marked as “sat’d”, which were measured in solutions saturated with FeCO₃. Rotating cylinder electrode, 1900 RPM. X65 steel except where noted. The pit penetration rates were measured on top of the general corrosion.

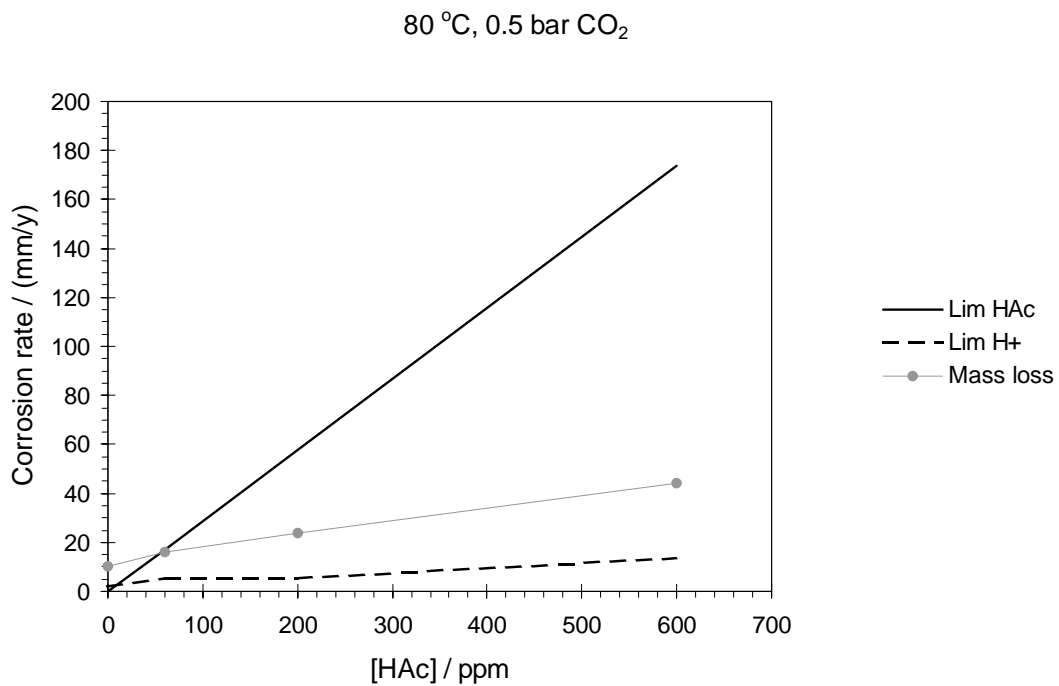
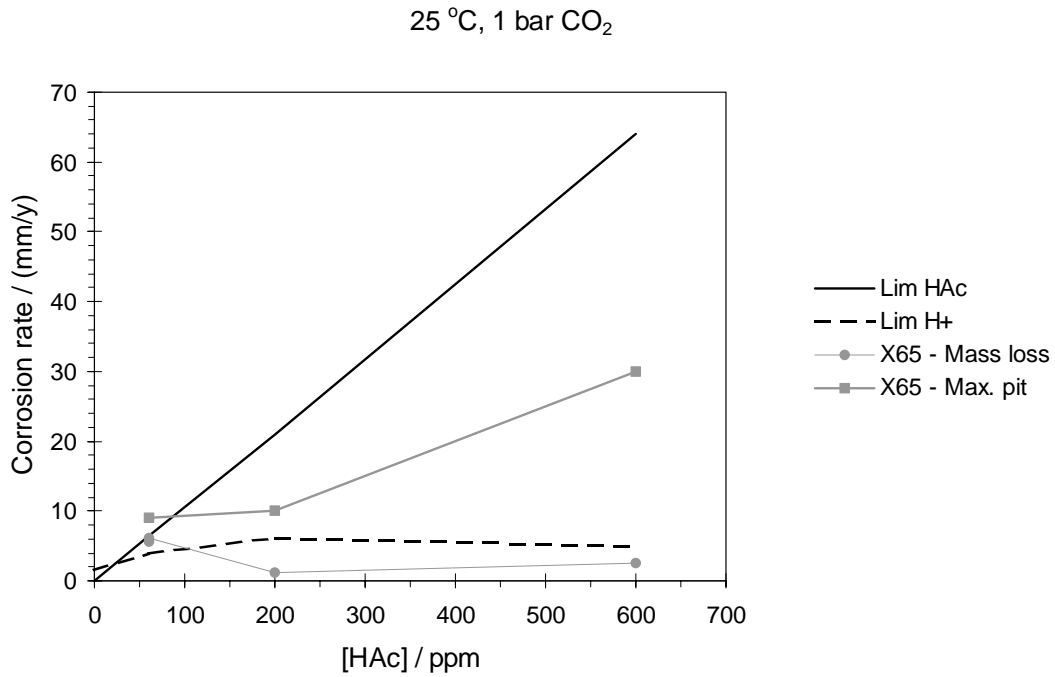


Figure 10 Diffusion limit of HAc and free H⁺ reduction at 1900 RPM expressed as corrosion rate (1 A/m² ≈ 1 mm/y). The main results of Figure 36 are also included for comparison. The calculations were based on the mass transfer correlation of Ref. 50, and diffusion coefficients were taken from Refs. 33-34, extrapolated to 80 °C by use of the Stokes-Einstein relation.⁴³ The H⁺ limits were calculated using the actual bulk pH in the tests.

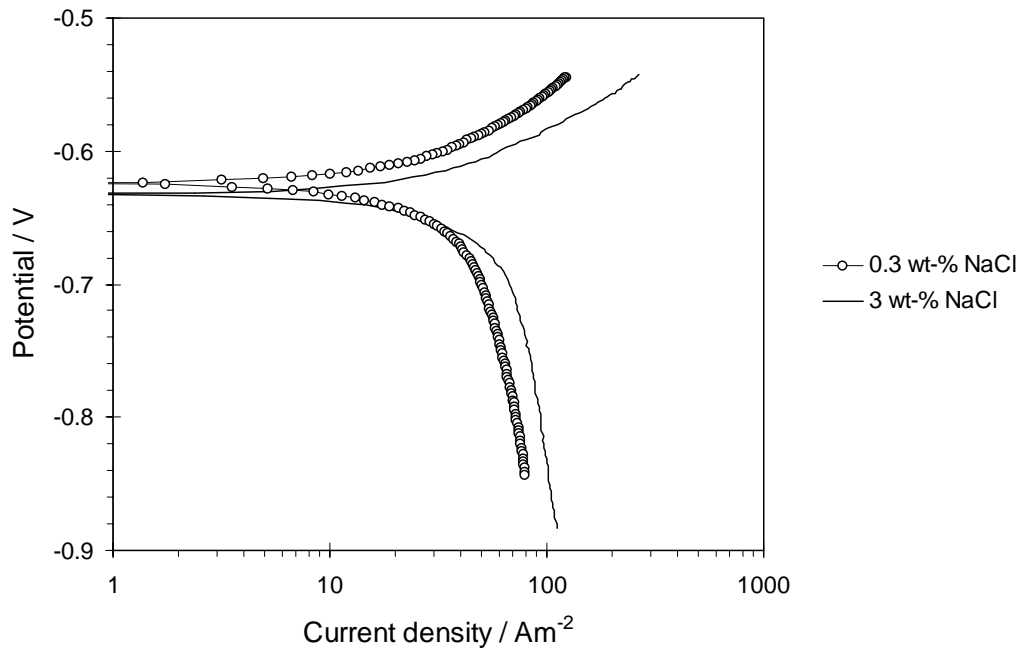
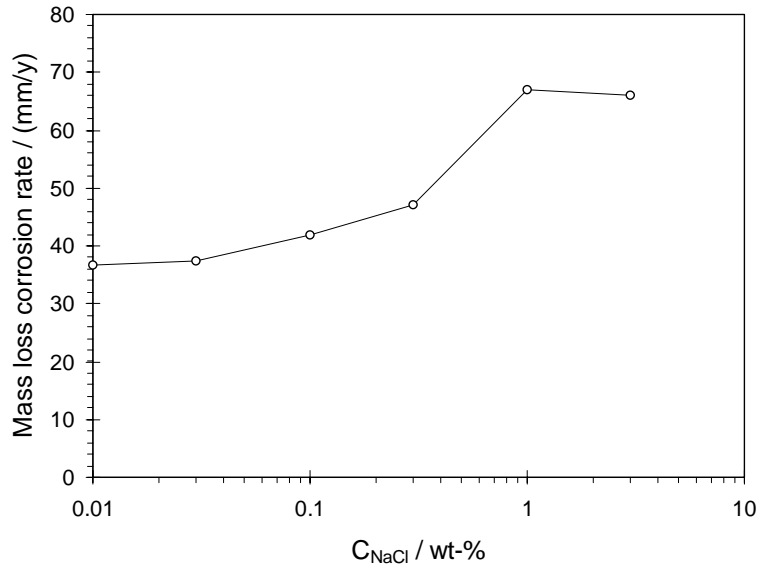
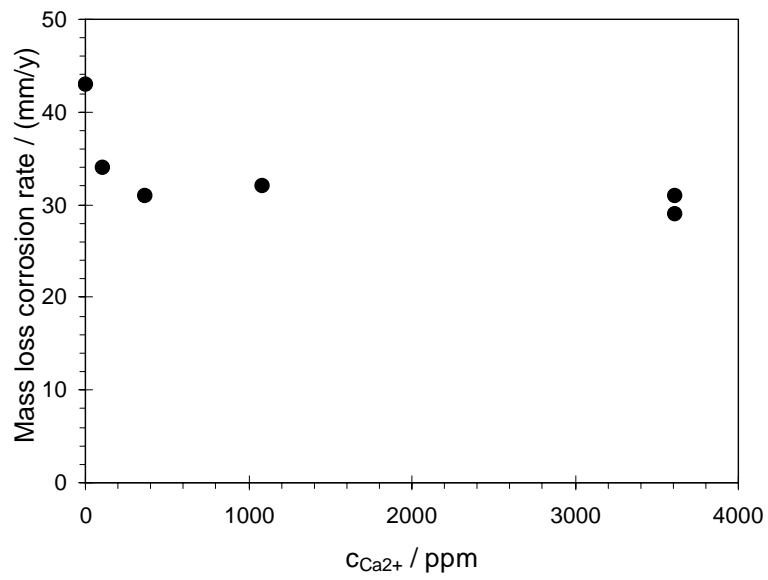
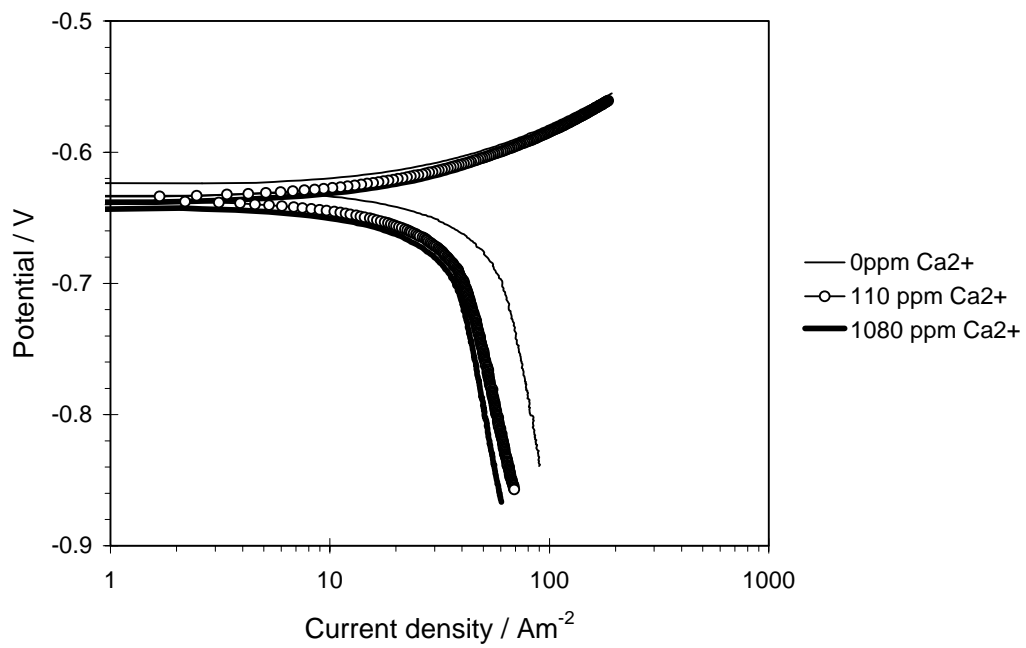


Figure 11 (a) Mass loss corrosion rate vs. NaCl concentration. (b) Potentiodynamic polarization curves at 0.3 wt-% and 3wt-% NaCl measured at the end of the tests in (a). Test conditions: 80 °C, 0.5 bar CO_2 , 200 ppm (3.33 mM) HAc added, pH 3.5-3.7.

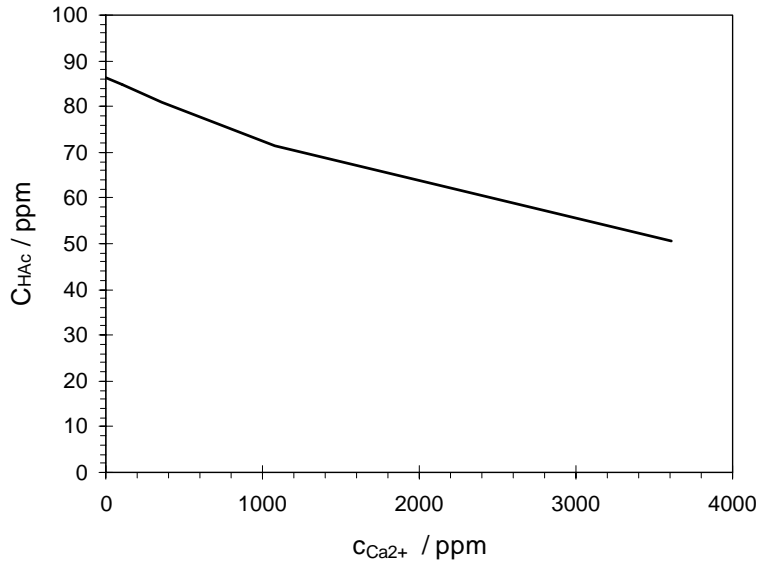


(a)



(b)

Figure 12a-b Caption overleaf



(c)

Figure 12 (a) Mass loss corrosion rate vs. total concentration of Ca^{2+} ions.
 (b) Potentiodynamic polarization curves measured at the end of the tests in (a).
 (c) Concentration change of undissociated HAc vs. total concentration of Ca^{2+} ions caused by formation of $CaAc^+$, according to Eq. 12. A complex formation constant of 14 was used, interpolated from data in Table 4 and corrected with activity coefficients estimated by means of the Davies equation.⁵⁹ Test conditions: 80 °C, 0.5 bar CO_2 , 200 ppm total acetate, 3 wt-% NaCl brine, pH adjusted to 4.6. 1900 RPM.